THE ASTROPHYSICAL JOURNAL, 324:974–994, 1988 January 15

THE ATMOSPHERIC STRUCTURE OF THE O-TYPE SUPERGIANT KRZEMIŃSKI'S STAR AND THE MASS OF ITS COMPANION NEUTRON STAR CENTAURUS X-3

GEORGE W. CLARK, JOSEPH R. MINATO, AND GUOZHU MI[1]
Department of Physics and Center for Space Research, Massachusetts Institute of Technology
Received 1986 October 3; accepted 1987 July 6

ABSTRACT

We find direct evidence of a coronal layer at the base of the supersonic wind of the O-type supergiant Krzemiński's star (KRZ) in X-ray observations of numerous eclipse ingresses and egresses of its companion X-ray pulsar Cen X-3. The characteristic shape and energy dependence of these X-ray eclipse transitions can be accounted for by a hybrid corona wind model of the KRZ atmosphere in which the wind is accelerated initially by the thermal pressure gradient in a thin coronal layer and then to hypersonic velocities by radiation pressure in the region beyond. We deduce from our data a smaller value of the eclipse half-angle than has been used in previous analyses of the orbital dynamics of the binary and derive from it a larger estimate of the neutron star mass, viz. $1.23 \pm 0.60\ M_\odot$.

Subject headings: stars: coronae — stars: eclipsing — stars: individual (Cen X-3) — stars: neutron — stars: winds — X-rays: binaries

I. INTRODUCTION

The gradual occultations of the binary X-ray pulsar Cen X-3 by its massive companion, KRZ, offer an opportunity to measure quite directly the structure of the extended atmosphere of an O-type supergiant which, like other stars of its type, emits a supersonic wind with a substantial rate of mass loss. In the high intensity state of Cen X-3 the eclipse transitions last ~80 minutes or 10° of orbital phase, and they provide, in effect, profile views of the atmosphere of KRZ from the region where the radial flow begins through a portion of the radiation-driven supersonic flow. There is clear evidence in the characteristics of the X-ray pulsations both out of eclipse and during eclipse transitions that the size of the illuminating source, i.e., the neutron star and possibly some portion of its accretion disk, is small compared to the scale height of the occulting atmosphere. Moreover, the geometry is "good" in the sense that nearly all of the detected X-rays come directly from Cen X-3. Thus the variation of X-ray intensity during an eclipse ingress or egress provides a direct measure of the column density along the line of sight through the KRZ atmosphere as a function of orbital phase. One can therefore test models of the atmosphere by comparing the observed eclipse transition curves with theoretical curves calculated from trial density functions.

We observed numerous eclipse transitions of Cen X-3 over the energy range from 1.5 to 20 keV with X-ray detectors on *SAS 3* during two extended periods when Cen X-3 was in its high-luminosity state. From the data we have inferred information about the radial distribution of the density in the atmosphere of KRZ and, by implication, about the temperature and the acceleration processes of its wind. We have also derived a smaller value for the eclipse half-angle than has been used in previous analyses of the orbital dynamics of the system. With this smaller value we obtain a significantly larger estimate of the mass of Cen X-3, thereby reducing the apparent anomaly in the Cen X-3 mass and moving it closer to the center of the distribution of other estimated masses of neutron stars in binary systems which cluster around the Chandrasekhar mass.

Cen X-3 was discovered in a rocket observation by Chodil *et al.* (1967). With the *Uhuru* satellite it was located precisely and found to be an eclipsing binary X-ray pulsar with a massive companion (Giacconi *et al.* 1971; Schreier *et al.* 1972). The latter authors observed that the eclipse transitions are gradual, and they characterized the atmospheric structure of the occulting primary by a "scale height" of 5×10^{10} cm. The system has since been studied extensively in X-rays (see review by Rappaport and Joss 1983). Its properties and those of KRZ are summarized in Table 1.

Krzemiński (1973, 1974) identified the optical counterpart of Cen X-3 as a highly reddened early-type star (KRZ) with a visual magnitude of 13.36 ± 0.06 and an ellipsoidal variation which coincides with the measured orbital motion of Cen X-3. Vidal *et al.* (1974) found P Cygni profiles in Hβ and He II λ4686 from which they deduced the presence of a stellar wind with a velocity of ~800 km s^{-1}. Rickard (1974) noted the absence of Hβ and He II lines in spectra taken 2 months earlier. Hutchings *et al.* (1979) detected Hβ and He II lines, but no P Cygni profiles at a time when simultaneous satellite observations showed that the X-ray source was in a high-luminosity state. However, they did find evidence in a velocity progression of ionic composition for a "mild" wind with a mass-loss rate of $\sim 5 \times 10^{-6}\ M_\odot\ \mathrm{yr}^{-1}$. They characterized KRZ as an evolved star of type O6–O8(f). Considering the extensive evidence for substantial winds in massive OB stars in general, the somewhat spotty evidence for such a wind in KRZ in particular, and the X-ray phenomenology of Cen X-3, it seems safe to assume that KRZ does indeed have a substantial and variable wind. Unfortunately, the large interstellar absorption along the line of sight to the binary system makes observation of the wind-diagnostic resonance absorption lines in the UV impossible.

The X-ray brightness and spectrum of Cen X-3 undergo large changes on a time scale of months. These have been identified by Schreier *et al.* (1976) as transitions between a state of high Eddington-limited X-ray luminosity to a state of low luminosity caused some times by "starvation" of the accretion process through a reduction in the flow of material from the

[1] On leave from the Nanjing Aeronautical Institute, Nanjing, China.

TABLE 1

PROPERTIES OF CENTAURUS X-3/KRZ SYSTEM[a]

Parameter	Value
Cen X-3:	
Pulsed fraction	0.45–0.56
Pulse period P_{pulse}	4.84 s
Orbital period P_{orb}	2.087 day
$a_x \sin i$	$(1.1926 \pm 0.0002) \times 10^{12}$ cm[b]
Eccentricity	0.0008 ± 0.0001
Mass function $f(M)$	$15.5\ M_\odot$
Inclination i	$>63°$
Eclipse half-angle θ_e	35°–40°[b] (32°.9)
KRZ:	
Spectral type	O6.5 II–III
K_c	24 ± 6 km s^{-1} [b]

[a] All values from Rappaport and Joss 1983 except spectral type from van Paradijs 1983, pulsed fraction from Ulmer 1976, and new eclipse half-angle in parentheses from this paper.

[b] Values used in the Monte Carlo analysis of the neutron star mass by Rappaport and Joss 1983.

primary, and other times by "smothering" of the X-ray emission by excessive flow. Spectral changes are accounted for as absorption by circumsource material. In its high state, or during episodes of partial starvation, the amplitude of the uneclipsed pulse-averaged X-ray spectrum of Cen X-3 is variable on a time scale of minutes but is fairly constant in shape except in occasional semiregular preeclipse dips. The latter appear to be caused by absorption in features of the accretion flow that pass in front of the source. Aside from these dips, the low-energy cutoff in the spectrum during the high-luminosity state indicates absorption by $\sim 3 \times 10^{22}$ H atoms cm^{-2} of matter with normal cosmic abundances, a quantity consistent with the strong reddening of the KRZ optical spectrum and therefore attributable primarily to interstellar matter.

Rocket and satellite observations of the P Cygni profiles of resonance absorption lines in the UV spectra of OB giants and supergiants revealed the existence in such stars of intense winds with supersonic velocities up to 3000 km s^{-1}, giving mass-loss rates estimated to be in the range from 10^{-7} to 10^{-5} $M_\odot$ yr^{-1} (Morton 1967; Lamers and Morton 1976; Conti and Garmany 1980). Radio continuum measurements (Abbott *et al.* 1980) and infrared measurements (Barlow and Cohen 1977) confirmed the existence of high rates of mass loss and yielded estimates that agree in general within factors of 3. The temperatures in the winds, derived from their ionic compositions, are much too low ($\sim$30,000–40,000 K) for acceleration by thermal pressure gradients alone to yield such high mass-loss rates. Lucy and Solomon (1970) suggested that the accelerating force arises from the scattering and absorption of UV radiation in resonance lines, and since then the theory of radiatively driven winds in early-type stars has been extensively developed (e.g., Castor, Abbott, and Klein 1975). The key idea of the theory is that the radiation force on any given shell of material moving outward with increasing supersonic velocity is maintained by virtue of the increasing Doppler shift of the absorption profiles toward shorter wavelengths and away from the spectral shadow of the material closer in.

Marlborough and Roy (1970) pointed out that radiation force, equal to or exceeding the gravitational force, cannot drive an initially subsonic flow to supersonic velocities. Hearn (1975) proposed that the initial acceleration occurs in a thin hot ($\sim 10^6$ K) coronal layer at the base of the wind, and that radiation pressure takes over at the top of this corona where the heating action terminates and the wind cools, leaving the flow velocity supersonic at the lower velocity. The existence of such a coronal layer with its X-ray emission offers the prospect of explaining the observed superthermal ionization in the winds of OB stars (Cassinelli, Olson, and Stalio 1978), and the observed fluxes of soft X-rays that typically comprise $\sim 10^{-7}$ of their total radiative luminosity (Cassinelli *et al.* 1981). Cassinelli and Olson (1979) worked out a more detailed theory of a "corona plus cool wind model" which accounts for the superthermal ionization but gives too small a flux of soft X-rays due to absorption of the coronal emission by the overlying material in the wind region. Waldron (1984) developed a "recombination stellar wind model" in which detailed consideration is given to the effect of the coronal soft X-ray emission on the temperature and velocity structure of the radiatively driven region. His theory predicts soft X-ray fluxes in agreement with those observed.

One problem with the idea that there is a coronal layer at the base of the stellar wind in an OB star is the lack of a detailed explanation of how such a layer is maintained at a million degree temperature in the presence of the rapid radiative cooling caused by its comparatively high density. Models have been advanced to explain the soft X-rays from single OB stars as the emission of shock-heated filaments or blobs produced by instabilities in the radiation-driven wind itself and carried along with it (e.g., Nelson and Hearn 1978; Lucy and White 1980), but such processes presumably operate only in the region above the base-corona layer.

Reviews and discussions of observational and theoretical aspects of many of these issues can be found in the *Proceedings of the IAU Symposium 83* (Conti and de Loore 1979).

II. OBSERVATIONS

We observed Cen X-3 with the HTC and XTC detectors of the *SAS 3* X-ray Observatory during two extended periods of pointed-mode operation from 1976 November 29 through December 2, and from 1978 December 19 through 1979 January 9. The detectors were proportional gas counters with fillings of argon and xenon, beryllium windows, and coaligned tubular collimators with 1°.7 FWHM fields of view. Additional details are given by McClintock *et al.* (1976). Figure 1 shows plots of the effective area versus energy for each of the four channels used in this study as computed from data on the construction and testing of the counters before launch and from inflight calibrations based on observations of the Crab Nebula.

The counting rates measured during 15 eclipse transitions, with background subtracted and corrections made for collimator transmission, are plotted as functions of the orbital phase angle in Figures 2*a*–2*d*. The indicated errors are statistical only and do not include uncertainties of comparable magnitude in the background subtraction and collimator transmission corrections. Our analysis is based primarily on the data from channels HTCB and XTCA which had the best statistical accuracy and a substantial difference in their energy ranges. Data from channels HTCA and HTCC are shown in Figure 2 only when they are of sufficient quality to make possible interesting comparisons with channels HTCB and XTCA. The time gaps are due primarily to Earth occultations. The fitted curves superposed on the plots are discussed below.

Data on the pulsations recorded in the four energy channels before and during the eclipse transition labeled "OBS 4" are

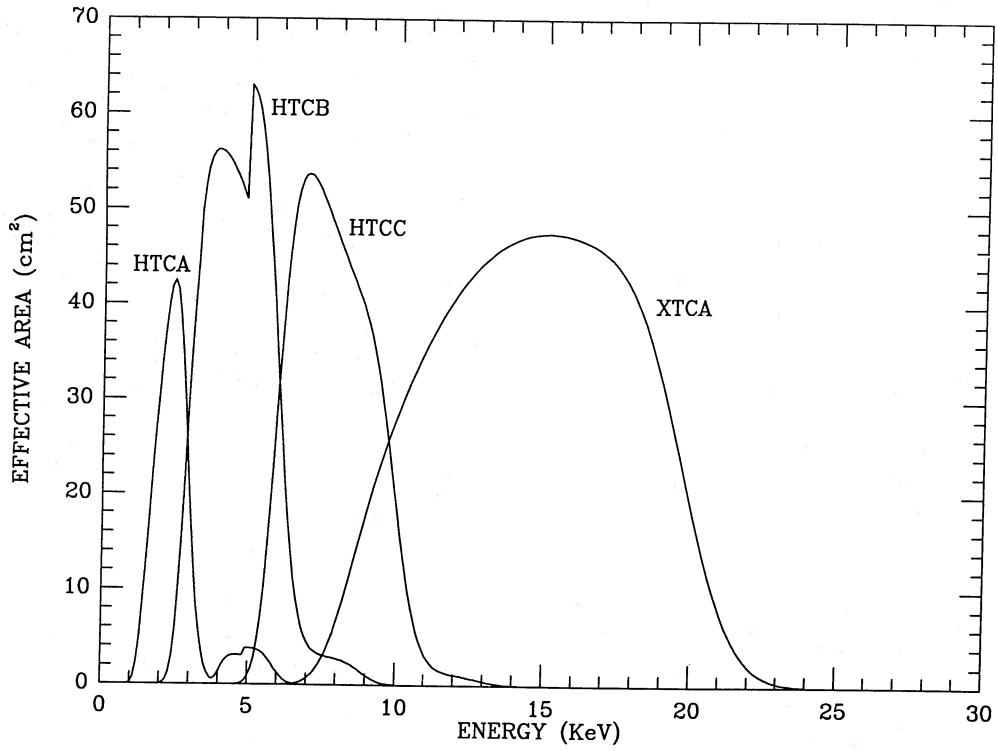

FIG. 1.—Effective areas of the detectors in four energy channels plotted vs. X-ray energy

displayed in Figure 3. The raw counts (detector background not subtracted) recorded during successive 0.01 day periods were binned in 0.8314 s intervals and folded modulo the pulse period of 4.83337 s. Plots in the first column of Figure 3 show the counting rates due to the completely uneclipsed Cen X-3 pulsed emission plus the detector background. The last column shows the pure background counting rates when Cen X-3 is completely eclipsed. Subtracting these background rates from each of the previous data sets, we find that the pulsed fractions in each of the four energy channels are in the range from 0.55 to 0.65 before the eclipse transition commences (col. [1]), and they do not change significantly during the eclipse transition (cols. [2]–[4]). Similar results are seen in all the other well-observed transitions. This implies that the variation of the pulsed intensity in each energy channel during the eclipse transitions is similar to the variation of the total intensity. We note with particular emphasis that the phase of the pulse peak does not vary by more than one 15° phase bin during the transition. We also note that the dependence on energy of the progress of the eclipse is evident in Figure 3: the pulsations disappear first in the low-energy channel and last in the high-energy channel as expected for an eclipse caused by photoelectric absorption in the atmosphere of the occulting star.

Figure 4 shows the ranges of possible angles from superior conjunction of the endpoints of the eclipse transitions for which data from the HTCB (*thin bars*) and XTCA (*thick bars*) channels are available. The even numbered transitions are ingresses and the odd numbered ones are egresses. The uncertainties in the end points are caused by missing data (generally due to Earth occultations), intrinsic intensity fluctuations, and counting statistics. The nonoverlap of several of the ranges indicates that there was a substantial degree of variability in the KRZ atmosphere during our observations. The chart shows a systematic shift toward zero orbital phase of the transition phenomena in the XTCA channel relative to the HTCB channel, attributable to the greater penetrating power of the higher energy X-rays detected in the XTCA channel. OBS 14 and 17 place the lowest upper limit (36°) on the phase angle at which the observed XTCA rate is significantly above its totally eclipsed value.

Plotted against one another in Figure 5 are the counting rates in the HTCB and XTCA channels at the high end of each of the 13 transitions for which we have good data from both channels. The highest and lowest counting rates differ by a factor of ~ 2. On the other hand, the ratio of the XTCA to HTCB rates, indicative of spectral shape, stays within a fairly narrow range, having a mean value of 0.59 with a standard deviation of 0.07.

III. ANALYSIS OF THE ECLIPSE TRANSITIONS

We consider first the possibility that the gradualness of the eclipse transitions is due to the spatial extension of the X-ray emitting region of Cen X-3. We take for granted the conventional idea that Cen X-3 is a neutron star with a strong magnetic field which has a dipole component inclined with respect to its rotation axis. Matter flowing to Cen X-3 from its giant companion is heated by conversion of its gravitational potential energy and is channeled by the magnetic field to the regions of the neutron star's magnetic poles where it radiates most of its energy as X-rays. The X-ray emission from such a region is anisotropic. Rotation of the star therefore causes a rotating beacon effect that modulates periodically the intensity of X-rays received at any distant point. The question is whether or not most of the beam is intercepted and scattered by gas in an extended region in such a way as to produce the appearance of an extended pulsar which undergoes gradual eclipse by a "hard edge" of the primary.

To cause all of the delay between onset of an eclipse tran-

1988ApJ...324..974C

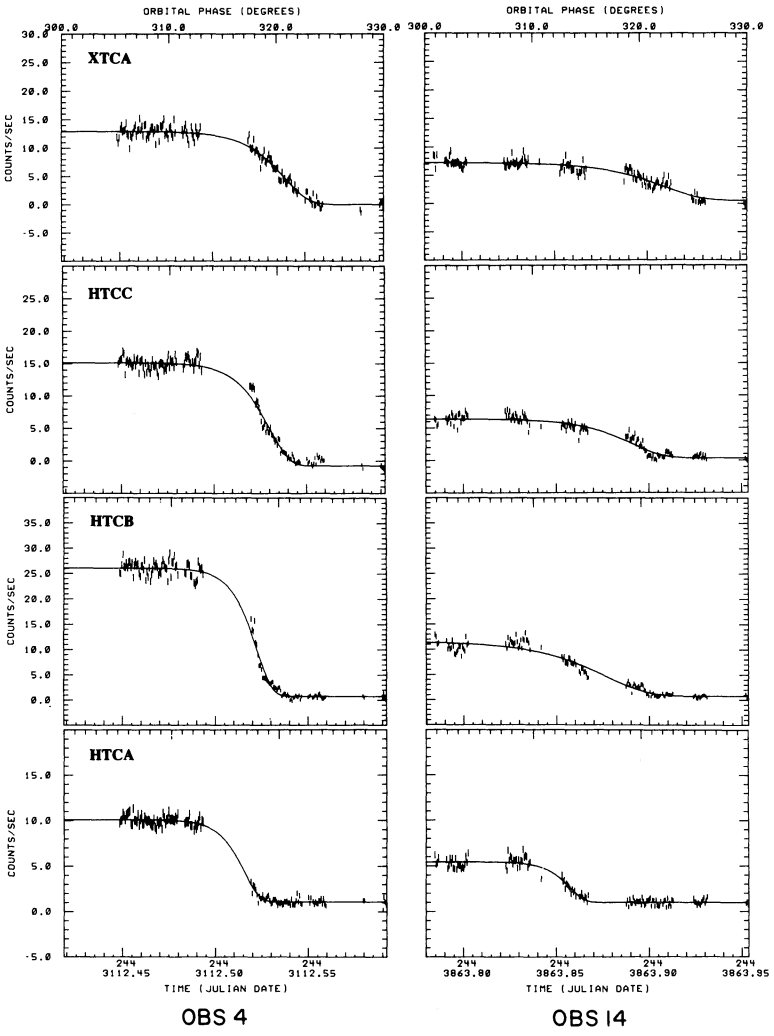

FIG. 2*a*

FIG. 2.—(*a*)–(*d*) Plots of the counting rates (background subtracted) against time in the various energy channels during observations of the eclipse ingresses and egresses of Cen X-3. Estimates of uncertainties due to counting statistics are indicated by vertical bars. Data indicated by filled triangles were omitted from the curve fitting because they appeared to be contaminated by unaccounted background fluctuations. Solid curves are the results of fitting the function defined by eq. (16).

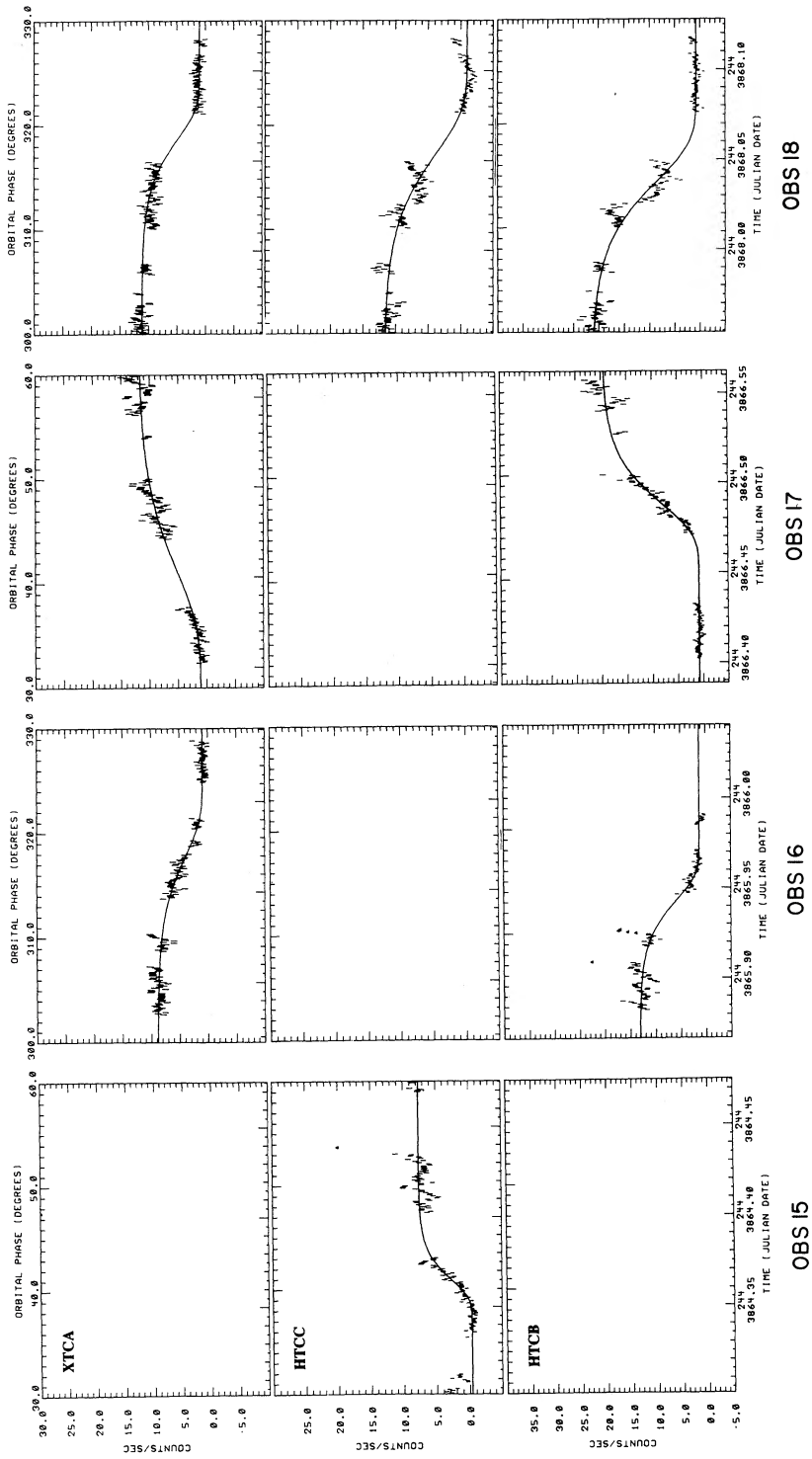

FIG. 2b

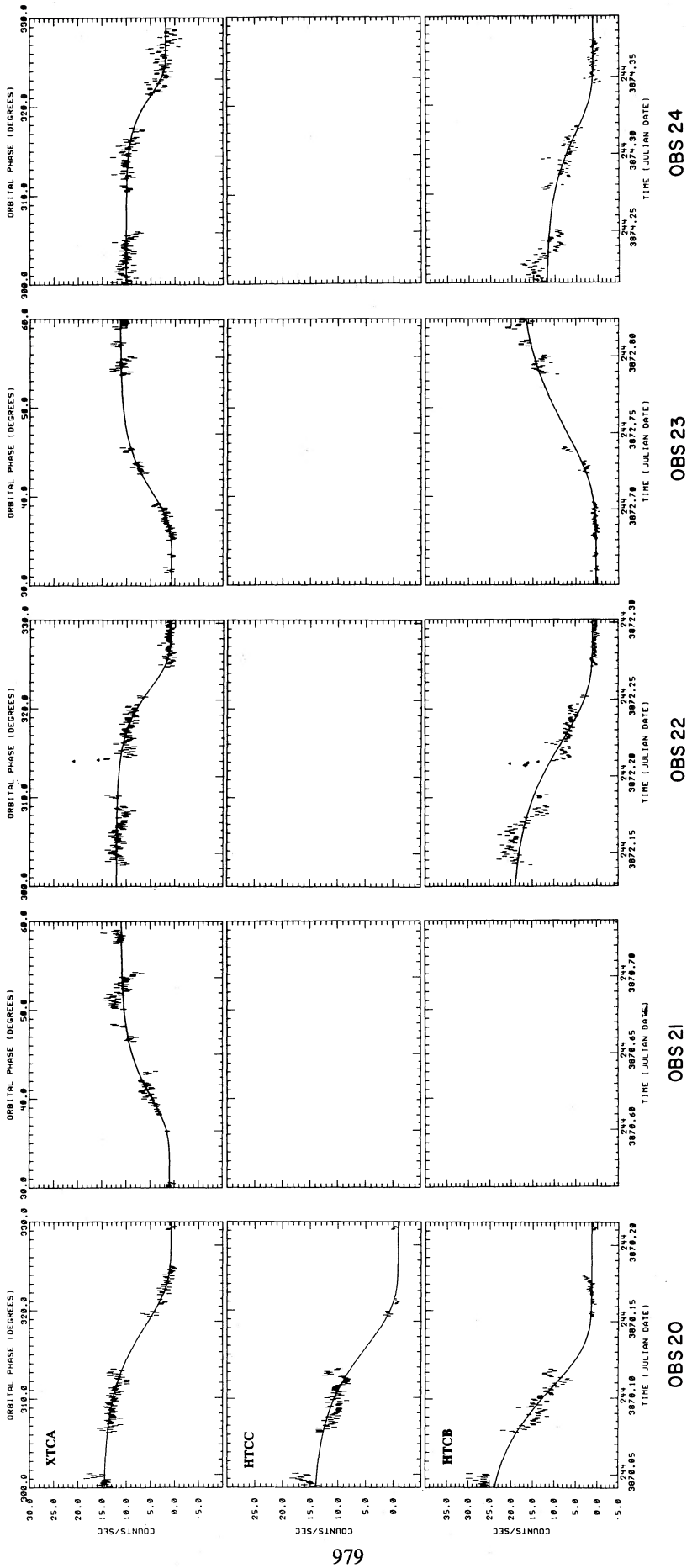

FIG. 2*c*

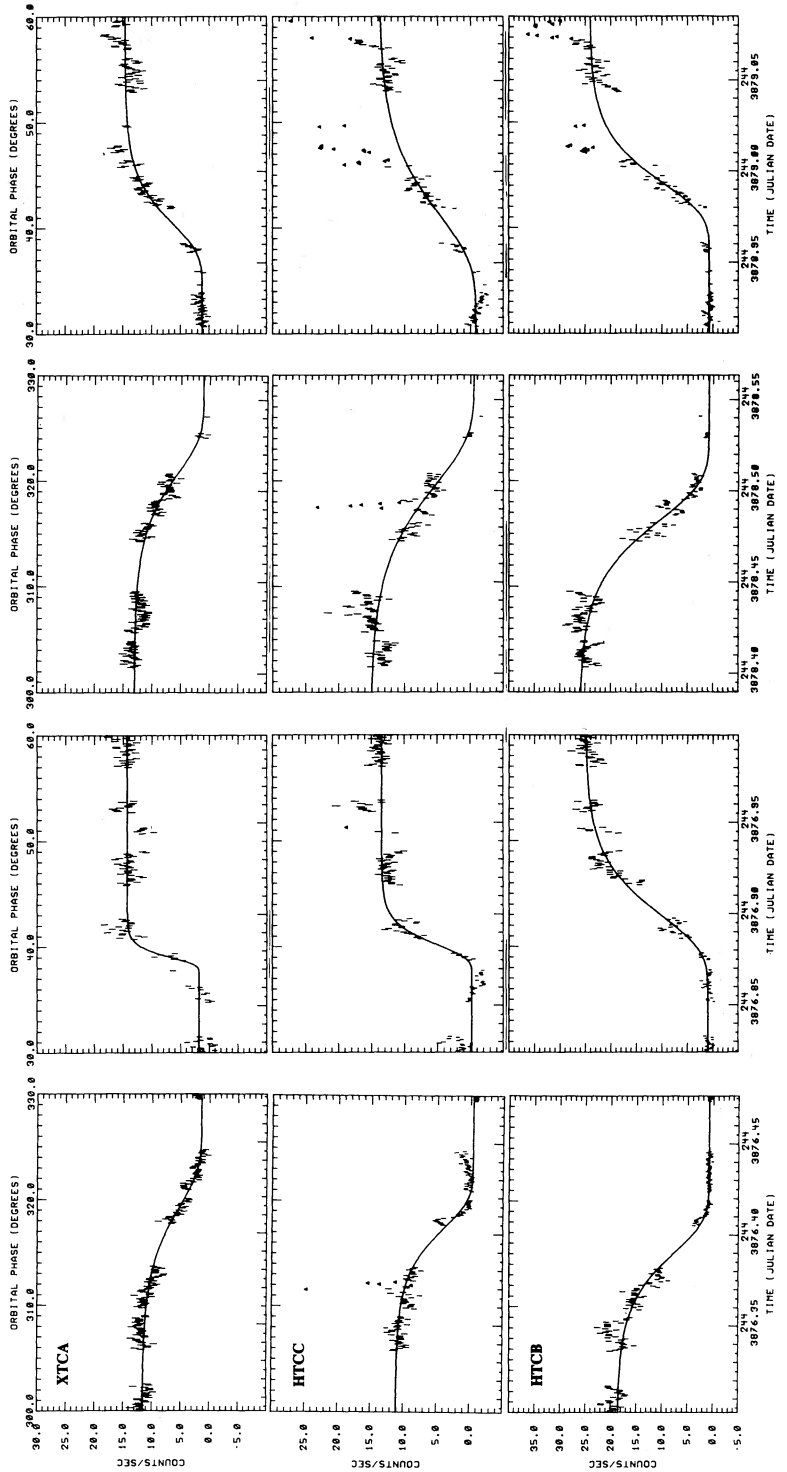

FIG. 2*d*

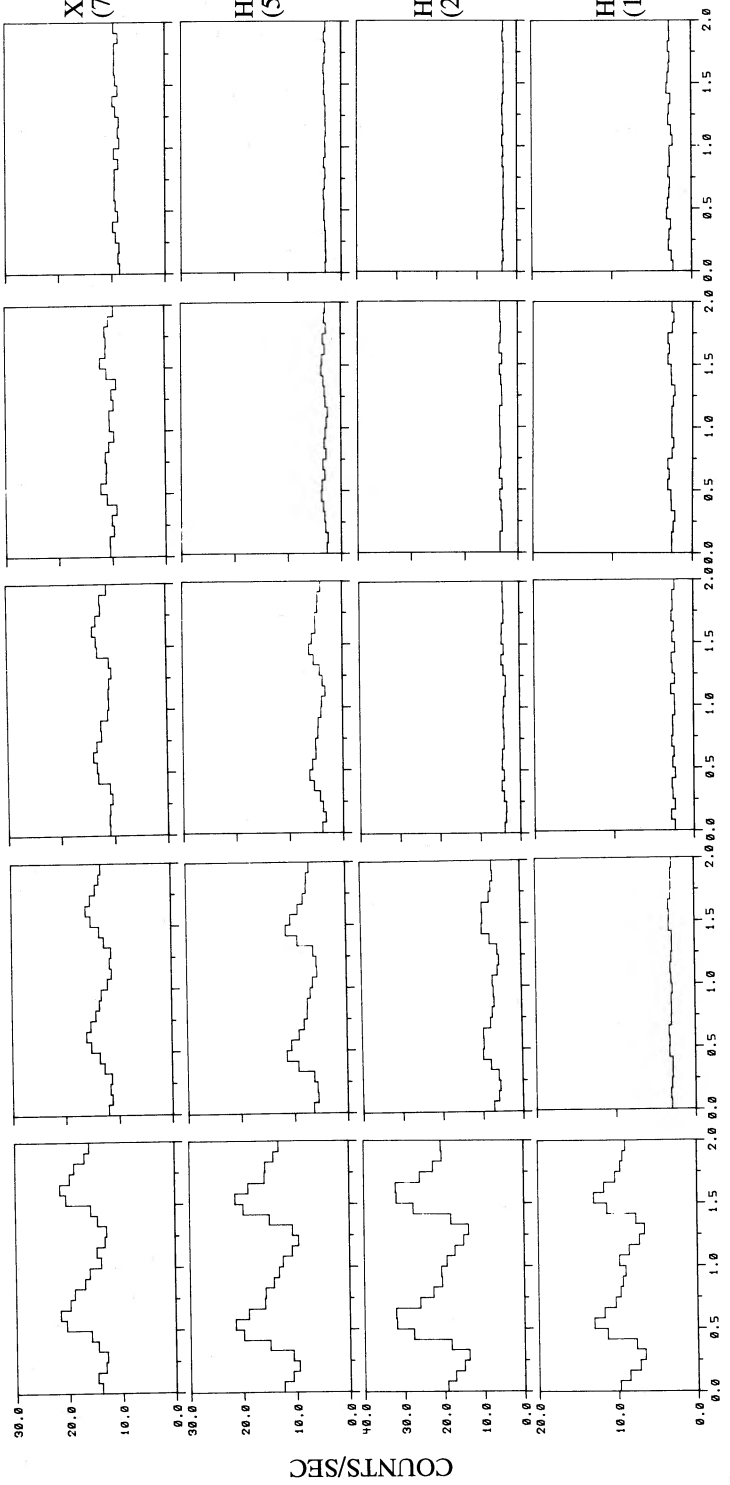

FIG. 3.—Pulsar light curves averaged over 0.01 day intervals just before (first column of panels) and during (next three columns) the OBS 4 eclipse transition. The data (detector background not subtracted) were binned in 0.83247 s intervals and folded modulo 4.83337 s. The background rates are indicated in col. (5) which displays the data recorded when Cen X-3 was completely eclipsed in all energy channels. The Julian time intervals are indicated above each column. The pulsed fractions of Cen X-3 radiation (background subtracted) in the four energy channels were in the range 0.55–0.65 both before and during the transition. Plots also show that the angle of Cen X-3 from superior conjunction to the point in orbit where its pulses are completely eclipsed decreases systematically with increasing energy of the X-rays as expected for attenuation due primarily to photoelectric absorption in the atmosphere of the primary.

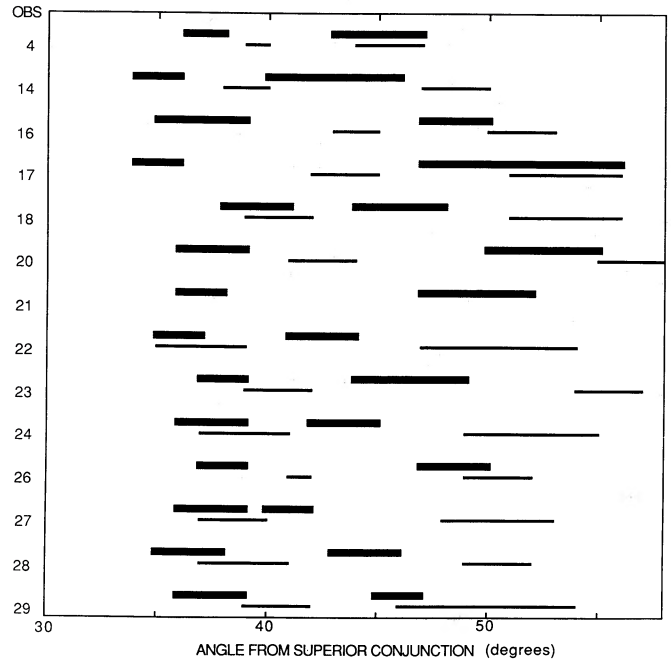

FIG. 4.—Chart showing ranges of possible beginning and end phases of eclipse transitions. HTCB data are indicated by thin bars and XTCA data by thick bars.

sition at orbital phase angle θ_1 and completion at $\theta_2 = \theta_1 + \Delta\theta$, the total width w of the extended emitting region in light-seconds must be

$$w \approx (a/c) \cos [(\theta_1 + \theta_2)/2]\Delta\theta , \quad (1)$$

where a is the distance between the centers of KRZ and Cen X-3 and c is the speed of light. Taking typical values of $\theta_1 = 37°$ and $\Delta\theta = 10°$, with $a = 1.3 \times 10^{12}$ cm, we find $w = 5.6$ lt-sec, which exceeds the distance traveled by light in one pulse period.

Cen X-3 undoubtedly has an accretion disk which intercepts and reradiates some portion of the X-rays generated near the neutron star. Evidence for the existence of large Compton thick accretion disk coronae, capable of diffusing a substantial portion of the primary X-ray emission of the neutron star, has been found in the partial X-ray eclipses of several nonpulsating accretion-powered binary X-ray sources by White and Holt (1982). However, we have not been able to imagine a plausible model of Cen X-3 in which a plasma cloud of diameter ~ 5.6 lt-sec, illuminated by a rotating beacon of X-rays emitted close to the magnetic poles of the neutron star, would be seen to pulsate coherently with a 4.84 s period, a pulse fraction of 0.5–0.6, and a phase that remains unchanged through eclipse transitions. We therefore reject the possibility that the gradual eclipses of Cen X-3 are due to the spatial extension of the X-ray source. Instead, we turn to an interpretation of the data based on the assumption that the gradual transitions are occultations of a point source of X-rays by the extended atmosphere of the primary.

We begin by deriving a function which can be fitted to the observed variations of counting rates versus orbital phase during the eclipse transitions. We then show that this function conforms to a theoretical transition function calculated for a hybrid model of an expanding atmosphere consisting of a high-temperature coronal layer beneath a cool stellar wind of the kind expected in a star of the type and class of KRZ.

We express the counting rate $C_j(\theta)$ at orbital phase angle θ in the jth energy channel by the equation

$$C_j(\theta) = \int_0^\infty I(E) \exp [-t(E, \theta)] A_j(E) dE , \quad (2)$$

where $I(E)dE$ is the unattenuated intensity of X-ray photons of energy E in dE from Cen X-3 and $A_j(E)$ is the effective area of the detector for detection of X-rays in the jth channel. The exponential factor represents the transmission along the line of sight through the KRZ atmosphere. The optical (i.e., X-ray) thickness is given by the path integral

$$t(E, \theta) = \int_{z_c}^\infty \sigma(E, z) n(z) dz , \quad (3)$$

where $\sigma(E, z)$ is the attenuation cross section per proton in the KRZ wind at the position z along the line of sight, $n(z)$ is the proton density, and z_c is the position of Cen X-3, as illustrated in Figure 6. We take $z = 0$ at the point along the line of sight nearest to the center of KRZ (i.e., the tangent point), so that

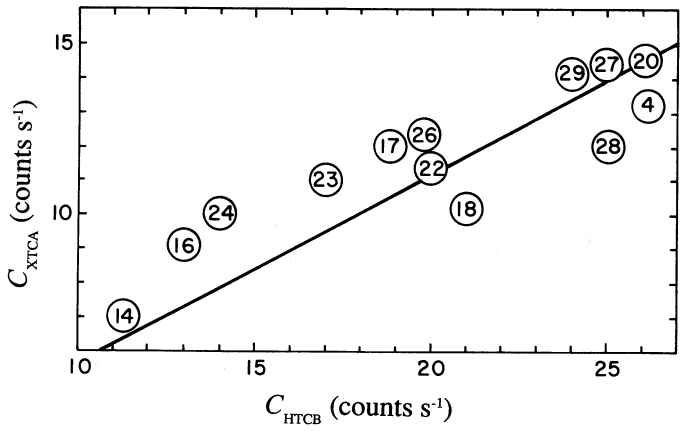

FIG. 5

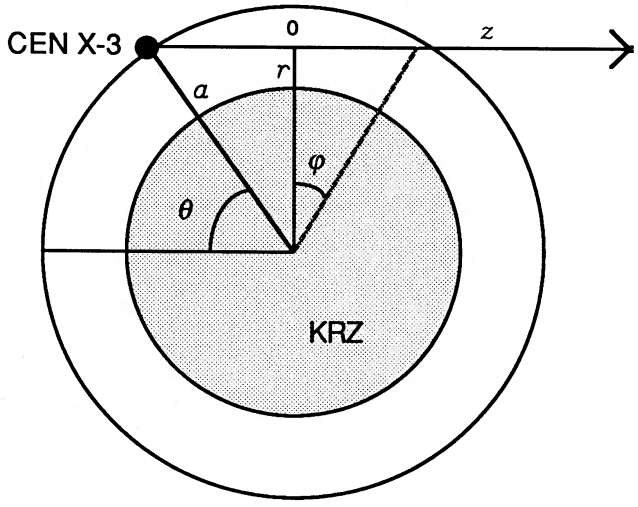

FIG. 6

FIG. 5.—Plot of the correlation between the uneclipsed counting rates in the HTCB and XTCA channels in the 13 observations identified by the OBS numbers in the data circles.

FIG. 6.—Illustration of the geometry for the model calculations of the X-ray attenuation along the line of sight to Cen X-3.

$z_c = -a \cos\theta \sin i$, where a is the distance between the centers of KRZ and Cen X-3 and i is the orbital inclination.

The X-ray intensities in the KRZ atmosphere are sufficiently high to cause substantial ionization and, consequently, to change the attenuation cross section per hydrogen atom along the line of sight. We will take this into account in the later calculations. However, for the sake of exploring the general character of the eclipse transitions we ignore for the moment the dependence of σ on z and set it equal to the total attenuation cross section for cold matter given by the expression

$$\sigma(E) = \sigma_{pe}(E) + 1.21\sigma_T , \tag{4}$$

where σ_{pe} is the photoelectric absorption cross section per hydrogen atom for interstellar matter with normal cosmic abundance as given by Morrison and McCammon (1983), σ_T is the Thomson scattering cross section, and the factor 1.21 is the number of electrons per proton in interstellar matter with normal cosmic abundances. Under this assumption the optical thickness at any given phase angle is proportional to the column density $N(\theta)$ at that phase angle, so that equation (3) can be written as

$$t(E, N) = \sigma(E)N . \tag{5}$$

Lacking detailed spectral information in the *SAS 3* data, we use for the spectrum the phase-averaged uneclipsed number spectrum derived by White, Swank, and Holt (1983) from multichannel proportional counter spectroscopy with *OSO 8* when Cen X-3 was in a high-intensity state like that which obtained during our observations, namely

$$\begin{aligned} I(E) &= I_0 E^{-\alpha} \exp\left[-\sigma(E)N_0\right] , \qquad E < E_c , \\ &= I_0 E^{-\alpha} \exp\left[(E_c - E)/E_f\right] \\ &\quad \times \exp\left[-\sigma(E)N_0\right] , \qquad E \geq E_c , \end{aligned} \tag{6}$$

TABLE 2

SUMMARY OF NOMINAL CHANNEL BOUNDARIES, EXPECTED COUNTING RATES PER UNIT I_0, AND EFFECTIVE ATTENUATION CROSS SECTIONS PER H ATOM OF COLD STELLAR MATTER

Channel	Nominal Energy Range (keV)	C_j/I_0 ($t = 0$) (cm^2 keV)	σ_j ($\times 10^{-24}$ cm^2)
HTCA	1.0–2.8	5.9	25.
HTCB	2.8–5.9	20.4	6.3
HTCC	5.9–10.0	14.2	2.5
XTCA	7.9–20.0	13.7	1.4

with $\alpha = 1.16$, $E_c = 11$ keV, $E_f = 8$ keV, and $N_0 = 3.0 \times 10^{22}$ H atoms cm^{-2}. With these assumptions equation (2) yields the unocculted counting rates per unit I_0 summarized in Table 2. The normalized attenuated rates plotted as functions of column density in Figure 7 where one can see that the logarithmic slopes of the calculated attenuation curves are fairly constant. The variations of the counting rates with column densities can therefore be represented with acceptable accuracy over the relevant range by the formula

$$C_j(N) = C_{j0} \exp\left(-\sigma_j N\right) , \tag{7}$$

with the effective cross sections defined by

$$\sigma_j = (1/N_{1/e})_j , \tag{8}$$

where $(N_{1/e})_j$ is the column density at which the counting rate in the jth channel is reduced by a factor of $1/e$. The effective cross sections, read from the intercepts of the curves with the $1/e$ abcissa, are also listed in Table 2.

We now assume that the density in the extended atmosphere of KRZ can be represented by a function of the distance from

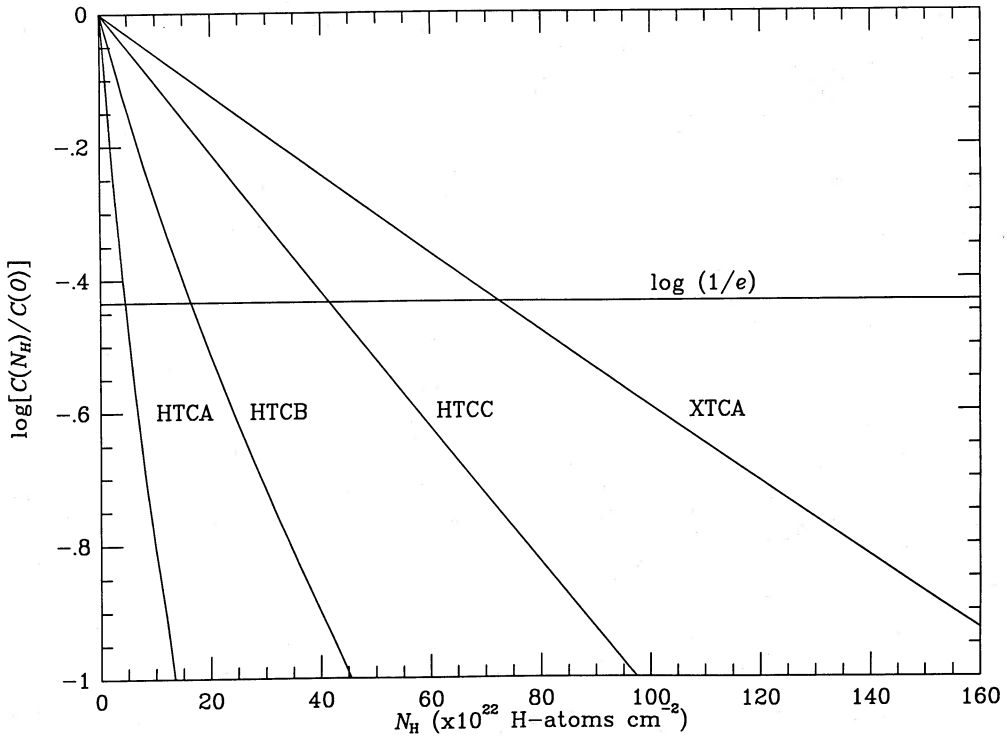

FIG. 7.—Calculated counting rates of Cen X-3 in the various energy channels plotted against the column density of interstellar matter with standard cosmic abundances.

the center of KRZ. We ignore the asymmetrical disturbances in the wind flow caused by X-ray–induced changes in the UV opacity which determines the local value of the radiation pressure (Fransson and Fabian 1980). We call $n(r)$ the number of protons per unit volume at radius r. The optical thickness for the jth channel along the line of sight is then

$$t_j = \int_{z_c}^{\infty} \sigma_j n(r) dz \, . \tag{9}$$

Given that the eccentricity of the orbit is negligibly small, we can write for the radial distance of a point at z along the line of sight to Cen X-3 at orbital phase θ the expression

$$r = a[(1 + \cot^2 \theta \cos^2 i) \sin^2 \theta + (z/a)^2]^{1/2} \, , \tag{10}$$

where z is measured from the point closest to the center of KRZ.

A visual survey of the eclipse transition data displayed in Figure 2 and those from other observations (e.g., *Uhuru*, Schreier *et al.* 1976; *Ariel 5*: Pounds *et al.* 1975; *COS B*, Bennett *et al.* 1976; Bonnet-Bidaud and Van der Klis 1979) shows that when Cen X-3 is "well fed" but not "smothered," the transitions (*a*) take place near an orbital phase of $\theta_c \sim 40°$ and over a phase interval of $\Delta\theta \sim 10°$, corresponding to a time interval of 1.3 hr; (*b*) are S-shaped, i.e., have rounded bottoms and tops; (*c*) show a progressive shift toward zero phase with increasing X-ray energy, but without substantial change of form. The gradualness of the eclipse transitions shows that densities of the order of $(\sigma a \sin \theta_e)^{-1} \approx 10^{12}$ cm^{-3} extend above the "surface" of KRZ to distances of the order of $a \cos \theta_e \Delta\theta \approx 2 \times 10^{11}$ cm. We will show that the energy-independent shapes of the transition curves and their energy-dependent shifts in orbital phase place constraints on the radial variation in the density of this extended atmosphere and limits on the mass-loss rate.

We note for future reference in the discussion of the Cen X-3 mass that the rounded bottoms of the transitions and the energy dependence of their phase indicate that the value of the eclipse half-angle which is appropriate for use in the conventional estimate of the neutron star mass may not be simply related to any obvious feature of a transition such as the "half-power" point, the baseline intercept of a line fitted to the steep portion of the transition, or perhaps not even the smallest phase angle at which a perceptible increase in X-ray intensity is observed. Thus a better understanding of the deep atmospheric structure of KRZ, derived from an interpretation of the eclipse transition data, should yield an improved estimate of the eclipse half-angle and the neutron star mass.

We have found that an exponential expression for the density

$$n(r) = n_0 \exp [-(r - r_0)/h] \, , \tag{11}$$

combined with the attenuation cross section for cold matter yields a function that can be satisfactorily fitted to the transition data. This density function, which happens to be that of an isothermal atmosphere in a uniform gravitational field, lends itself to a convenient analytical approximation when used in equation (9) to compute the optical thickness as a function of the orbital phase angle. Thus, in spite of its lack of apparent relevance to a central field, we have used it in our preliminary analysis of the data. To derive the approximation we change the variable of integration to φ by the substitution

$$z = a \sin \theta \tan \varphi \, , \tag{12}$$

and put $i = 90°$. Observing that the contributions to the integral come primarily from the narrow region along the line of sight close to the tangent point where $\varphi \ll 1$, we approximate sec φ by $(1 + \varphi^2/2)$ in the exponential factor of the integrand, and set $\sec^2 \varphi = 1$ in the differential. We also exploit the fact that the transition takes place over a small range of phase near θ_{0j} which we call the reference phase angle for the transition observed in the jth energy channel. For the reference radius we take $r_0 = r_{0j} = a \sin \theta_{0j}$. For angles close to θ_{0j}, equation (9) can then be written as

$$t_j(\theta) = \sigma_j n_0 a \sin \theta \exp [-(a/h)(\theta - \theta_{0j}) \cos \theta_{0j}] \times \int_{\varphi_c}^{\pi/2} \exp [-(a/h) \sin \theta(\varphi^2/2)] d\varphi \, , \tag{13}$$

Replacing the integral by its evaluation from $-\infty$ to $+\infty$, we obtain

$$t_j(\theta) = \sigma_j n_0 h[2\pi(a/h) \sin \theta]^{1/2} \times \exp [-(a/h)(\theta - \theta_{0j}) \cos \theta_{0j}] \, . \tag{14}$$

We now choose the reference radius to be at unit optical (i.e., X-ray) depth below the top of the atmosphere so that

$$n_{0j} \sigma_j h = 1 \, . \tag{15}$$

The expression for the counting rate in the jth channel is then

$$C_j(\theta) = C_{0j} \exp \{-[2\pi(a/h) \sin \theta]^{1/2} \times \exp [-(a/h)(\theta - \theta_{0j}) \cos \theta_{0j}]\} \, . \tag{16}$$

We have used the function defined by equation (16) to fit the data displayed in Figures 2*a*–2*d*, in each case fixing C_{0j} to match the uneclipsed rate and adjusting θ_{0j}, h, and the fully eclipsed counting rate to minimize χ^2. Occasional large deviations, in most cases due to unaccounted background fluctuations, are ignored in the curve fitting. The characteristic features of the eclipse transitions, listed above, are evidently fitted well by the formula. The fitted values of h (scale height) and θ_{0j} (reference angle) are listed in Table 3, and the correlations between the values from the two channels for which we have the most extensive data, i.e., HTCB and XTCA, are displayed graphically in Figure 8. The reference angle for the XTCA channel, which records the more penetrating X-rays, is systematically smaller than for the HTCB channel. The mean shift (excluding the apparently anomalous case of observation No. 27) in reference angle between these two channels is 4°.3. Although the fitted values of the scale height exhibit substantial scatter from one transition to another, the difference between the values for the HTCB and XTCA channels in each transition is generally small and not predominantly of one sign. Thus the scale height parameter appears to be an energy-independent measure of the structure of the atmosphere.

The fact that the reference angle changes systematically with the energy of the detected X-rays shows that much of the attenuation is caused by photoelectric absorption in matter with the K shells of the $Z > 2$ elements mostly intact. To compare the observed shift with the shift expected for attenuation in "cold" matter with an exponential density function we observe that the shift in the reference radius between the jth and kth channels is given by the equation

$$\delta r_0 = a(\sin \theta_{0j} - \sin \theta_{0k}) \approx a \cos \bar{\theta}_0(\delta\theta_0) = h \ln (n_{0k}/n_{0j}) \, , \tag{17}$$

TABLE 3

PARAMETER VALUES OF FITTED ECLIPSE TRANSITION CURVES

	SCALE HEIGHT ($\times 10^{10}$ cm)				REFERENCE ANGLE			
OBSERVATION	HTCA	HTCB	HTCC	XTCA	HTCA	HTCB	HTCC	XTCA
				Ingress				
04*	2.4	2.5	3.3	4.1	39°4	38°2	36°1	33°9
14*	2.2	7.1	5.3	6.6	42.8	35.1	34.3	30.5
16*	...	3.9	...	6.2	...	41.0	...	34.7
18*	...	6.4	7.5	5.2	...	37.4	34.2	34.8
20*	...	8.3	8.5	8.3	...	38.7	34.7	32.7
22*	...	10.2	...	5.8	...	33.2	...	31.0
24*	...	7.5	...	4.5	...	34.7	...	33.1
26*	...	5.2	5.2	6.4	...	38.0	36.0	33.3
28*	...	6.4	8.5	6.2	...	35.9	31.5	32.1
				Egress				
15	...	...	3.0	...	...	...	36.5	...
17*	...	4.9	...	10.0	...	40.2	...	31.1
21	...	...	...	6.7	...	...	...	32.6
23*	...	9.3	...	6.3	...	36.3	...	33.2
27	...	5.9	2.2	1.3	...	35.6	36.7	36.7
29*	...	5.1	8.3	5.0	...	37.3	32.3	34.1
Mean of*		6.4		6.2		37.2		32.9
Grand average			6.3				...	
Mean difference			...				4.3	

where $\bar{\theta}_0 = (\theta_{0j} + \theta_{0k})/2$ and $\delta\theta_0 = (\theta_{0j} - \theta_{0k})$. Substituting from equation (15), we obtain

$$\delta\theta_0 = (h/a \cos \bar{\theta}_0) \ln (\sigma_j/\sigma_k) . \quad (18)$$

Evaluating equation (18) for channels HTCB and XTCA with $h = (6.3 \pm 0.4) \times 10^{10}$ cm, $a = 1.3 \times 10^{12}$ cm, $\bar{\theta}_0 = 35°.1$, and $\sigma_{HTCB}/\sigma_{XTCA} = 4.5 \pm 0.5$ (from Table 2), we find $\delta\theta_0 = 5°.1 \pm 0°.7$, in satisfactory agreement with the average of the measured values.

IV. STRUCTURE OF THE KRZ ATMOSPHERE

We have shown that the eclipse transition curves are fitted well by equation (16), with average values of the fitted parameters for the XTCA channel being $\theta_0 = 32°.9$ and $h = 6.3 \times 10^{10}$ cm. According to equation (15), these values, together with $\sigma_{XTCA} = 1.4 \times 10^{-24}$ cm^2, imply a density of $n_0 = (1/h\sigma_{XTCA}) = 1.13 \times 10^{13}$ cm^{-3} at the reference radius $r_0 = a \sin 32°.9 = 7.06 \times 10^{11}$ cm. The HTCB transitions are also fitted well by equation (16) with the same value of h and $\theta_0 = 37°.2$, where the shift in orbital phase is attributable to the larger effective attenuation cross section for the X-rays detected in the HTCB channel.

There is no obvious physical significance to the simple exponential density function except its suggestive relation to an isothermal hydrostatic atmosphere in a uniform gravitational field. Moreover, our derivation of the approximate formula for the line-of-sight attenuation in an exponential atmosphere neglected the effect of X-ray–induced ionization on the photoelectric opacity of the attenuating matter. We will therefore use equation (16) with the average values of the fitted parameters only as a representation of the archetypal eclipse transition curves, and will seek a physically plausible atmosphere model with ionization which predicts eclipse transition curves that conform to the archetypal curves.

X-ray–induced change in the photoelectric opacity of the absorbing matter around KRZ was invoked qualitatively by

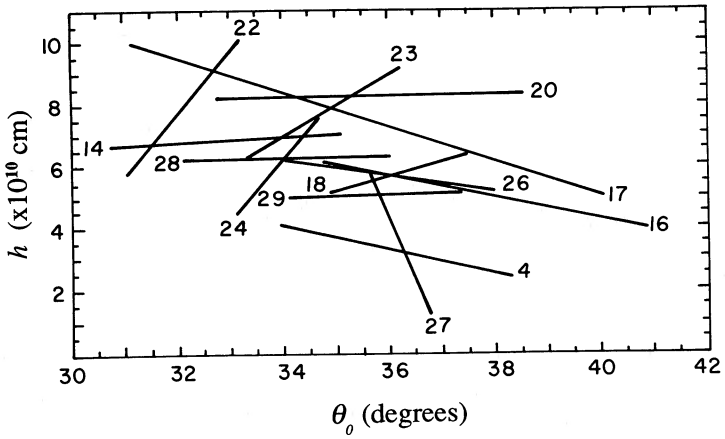

FIG. 8.—Comparisons of the fitted values of h and θ_0 for the 13 eclipse transitions observed in both the HTCB and XTCA channels. Except in the case of OBS 27 the right-hand end of each bar is the result for the HTCB channels, the left-end the result for the XTCA channel.

Schreier *et al.* (1976) and quantitatively by Hatchett and McCray (1977) to explain the phenomena observed during the transitions from the smothered low X-ray luminosity state to the high-luminosity state. The latter authors based their discussion on detailed calculations of the properties of X-ray irradiated plasma. Further extensive calculations of X-ray nebular models have been reported by Kallman and McCray (1982). Guided by their results, we have represented the effect of X-ray irradiation by Cen X-3 on the effective cross sections by the formula

$$\sigma'_j = 1.21\sigma_T + (\sigma_j - 1.21\sigma_T) \exp \{-\exp [(\log \xi - 3.2)/0.4]\} , \quad (19)$$

where $\sigma_T = 6.65 \times 10^{-25}$ cm^2 is the Thomson cross section and ξ is the ionization parameter L_x/nD^2. The exponential factor in the second term of equation (19) represents the ratio of densities of bare nuclei to total nuclei with $Z > 2$. Figure 9 is a plot of this formula for the ionization-modified attenuation cross section versus log ξ for the HTCB and XTCA channels.

To estimate the range of Cen X-3 luminosities we assume that the intrinsic source spectrum had the form specified by equation (6) throughout our observations and only varied in magnitude. We also assume that the exponential attenuation factor is absent in the intrinsic source spectrum of Cen X-3. Adjusting I_0 to convert the rates per unit I_0 listed in Table 2 into the ones observed, we estimate that the range of luminosities during our observations was

$$L_x = (1.1\text{–}2.6) \times 10^{38} (S/10 \text{ kpc})^2 \text{ ergs s}^{-1} , \quad (20)$$

where S is the distance to Cen X-3, for which values of 8 kpc (Krzemiński 1974) and 10 kpc (Hutchings *et al.* 1979) have been estimated. For L_x we adopt a value of 10^{38} ergs s^{-1}.

We now apply this ionization correction in a numerical calculation of the eclipse transition curves expected for a density function that is a solution of the hydrostatic equation for an isothermal atmosphere of ionized hydrogen in a central gravitational field; i.e.,

$$n(r) = n_1 \exp [-(r - r_1)/(r\tau^2)] , \quad (21)$$

where n_1 is the number density of protons at radius r_1, and τ is a temperature parameter defined by

$$\tau = [2kTr_1/G(1 - \Gamma)Mm]^{1/2} . \quad (22)$$

In this definition T is the kelvin temperature, M is the mass of the star, m is the proton mass, k is Boltzmann's constant, and $G(1 - \Gamma)$ is the gravitational constant multiplied by a factor representing the reduction in effective gravity due to radiation pressure. Since this density function approaches a finite value at large r, it describes the unphysical case of a static atmosphere confined to a star by a finite pressure at a large distance. In the absence of confinement the hydrostatic equation must be replaced by the hydrodynamic equations which describe an accelerating outward flow (Parker 1958, 1965). The density function in such a flow at constant temperature approaches equation (21) in the limit of a zero rate of mass loss. We first explore how closely the eclipse transition curves computed for the density function defined by equation (21) can be made to conform to the archetypal curves by adjustment of the temperature parameter τ.

For the effective luminosity L'_x at position z along the line of sight we use the intrinsic luminosity of Cen X-3 reduced by the accumulated attenuation factor; i.e.,

$$L'_x = L_x \exp \left(- \int_{z_c}^{z} \sigma'_j n dz \right) . \quad (23)$$

We integrated equation (9) numerically, using the hydrostatic

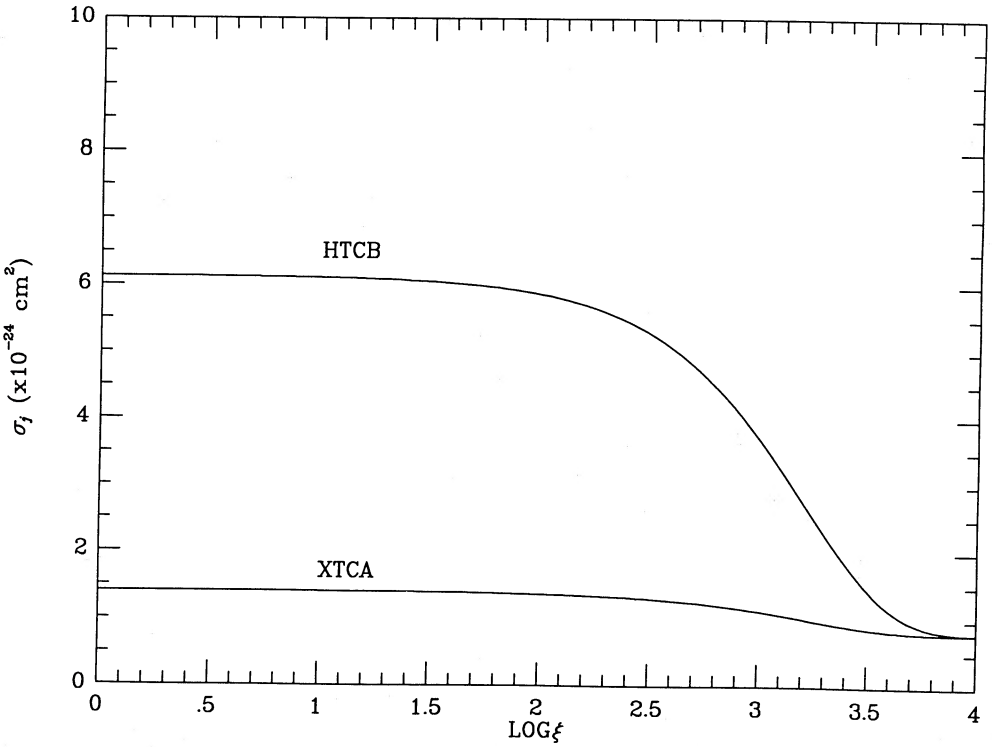

FIG. 9.—Plots of the attenuation cross sections used in the calculation of eclipse transitions plotted against the ionization parameter $\xi = L_x/nD^2$

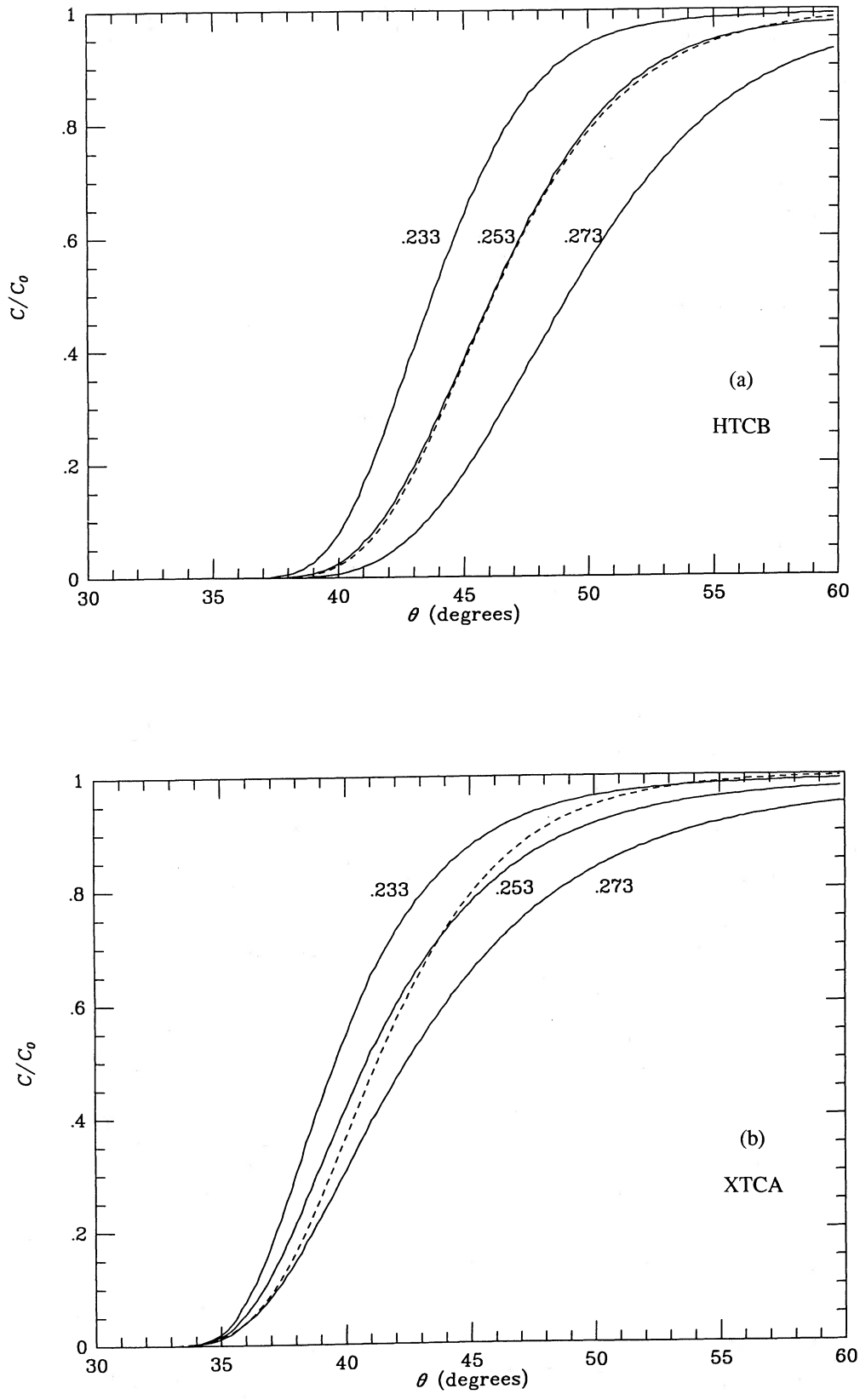

FIG. 10.—(*a*) Calculated eclipse transition curves (*solid lines*) for HTCB for hydrostatic, isothermal atmospheres for three temperatures and with ionization of the absorbing matter by X-rays from Cen X-3 at an assumed X-ray luminosity of 10^{38} ergs s^{-1}. Curves are labeled by the value of the temperature parameter τ. Dashed line is the archetypal curve for $\theta_0 = 37°.2$ and $h = 6.3 \times 10^{10}$ cm. (*b*) Same for XTCA, except $\theta_0 = 32°.9$. (*c*) Hydrostatic density functions for the three temperatures.

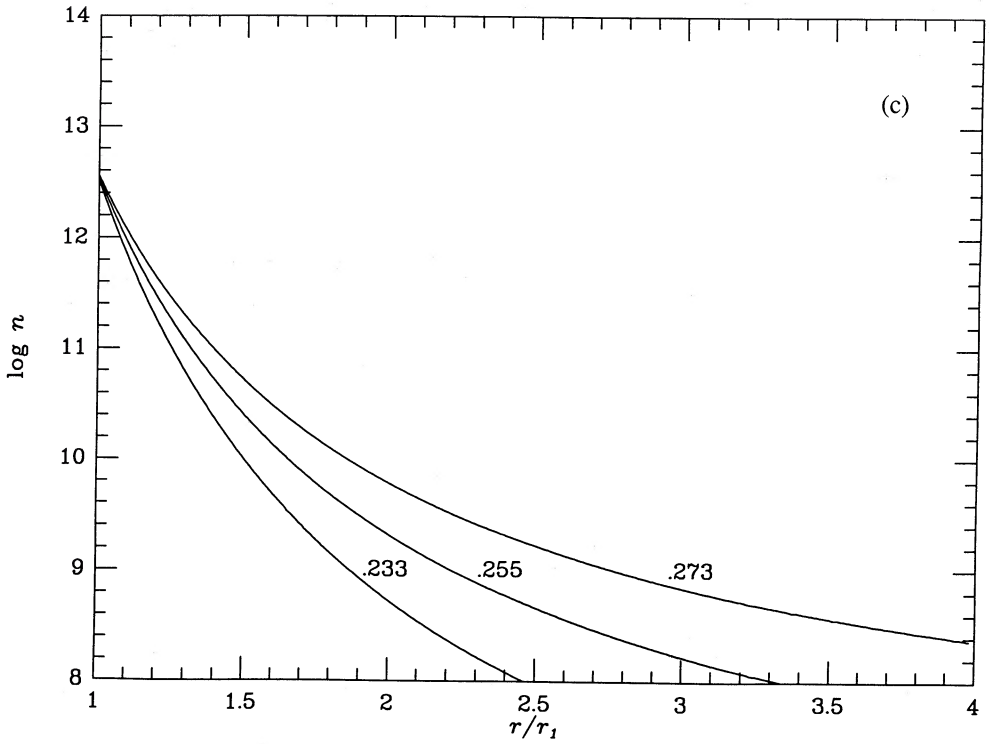

FIG. 10—*Continued*

density function specified by equation (21) with $n_1 = 4.5 \times 10^{12}$ cm^{-3} at $r_1 = a \sin 36° = 7.6 \times 10^{11}$ cm and the ξ-dependent cross sections of equation (19) with $L_x = 10^{38}$ ergs s^{-1}. Substituting the result in equation (2), we obtained the calculated eclipse curves shown in Figures 10*a* and 10*b* for values of $\tau = 0.233$, 0.253, and 0.273. The dashed curves are plots of equation (16) with $h = 6.3 \times 10^{10}$ cm, and with $\theta = 32\overset{\circ}{.}9$ and $37\overset{\circ}{.}2$ for the XTCA and HTCB channels, respectively. Good fits to the data for both channels are obtained for $\tau = 0.253$, corresponding to a kelvin temperature of $T = 1.3 \times 10^6(1 - \Gamma)$ K and to a scale height $\tau^2 r_1 = 4.9 \times 10^{10}$ cm. As one would expect, the scale height for the best fitting hydrostatic atmosphere is somewhat smaller than the scale height of the exponential fitting function. For $\Gamma \approx 0.5$ the implied temperature is high enough to qualify the atmosphere as a corona. Figure 10*c* shows plots of the hydrostatic density functions for the three values of τ.

Theories of radiation-driven supersonic stellar winds predict an accelerating force that varies approximately as $1/r^2$. The resulting velocity function has the form

$$v(r) = v_1\{1 + [(v_t/v_1)^2 - 1][1 - r_1/r]\}^{1/2}, \quad (24)$$

where v_1 is the velocity at r_1 and v_t is the terminal velocity. Combined with the equation of continuity, it implies the density function

$$n(r) = \dot{M}/[4\pi r^2 v(r)], \quad (25)$$

where $\dot{M}$ is the mass-loss rate.

We examine next the characteristics of the eclipse transition curves calculated for a wind in which the entire run of velocity is described by equation (24). To facilitate a comparison with the previous calculations we take n_1 and r_1 as in the hydrostatic case. We set the terminal velocity equal to 2000 km s^{-1}. Figure 11*c* shows the runs of velocity and density for various mass-loss rates in a range from $10^{-7.0}$ to $10^{-5.0}$ $M_\odot$ yr^{-1}. The various velocity curves are indistinguishable because in all cases $v_1 \ll v_t$; they resemble closely the curves displayed by various authors (e.g., Cassinelli and Olson 1979) in their discussions of radiation driven winds. Figures 11*a* and 11*b* show the calculated transition curves with ionization modeled for an X-ray luminosity of 10^{38} ergs s^{-1}. It is apparent that none of these curves is consistent in its shape and energy dependence with the observed transitions. In particular, if the mass-loss rate is high enough to produce a gradual rise in the HTCB curve as emersion begins or immersion ends, then both the HTCB and XTCA transitions extend over too large a range in orbital phase. Lower mass-loss rates produce initial rises which are too steep. And, perhaps most significant, the transition curves for any given mass-loss rate fail to show similar shapes in the HTCB and XTCA channels with the characteristic shift in orbital phase which is so prominent a feature of the data and which is embodied in the archetypal curves shown as dashed lines in the figure. These failures arise from the basic character of a radiation-driven wind which combines a high initial acceleration with an asymptotic approach to the terminal velocity at large distances. We conclude that a pure radiation-driven wind is not compatible with the eclipse transition data.

V. THE CORONA WIND MODEL

We now explore the implications of a hybrid corona wind model which we construct according to the following picture: we assume that thermal pressure causes the initial acceleration in a coronal layer of uniform high temperature at the base of the wind. At the point where the velocity approaches the speed of sound the coronal heating mechanism shuts off and rapid radiative cooling sets in, thereby converting subsonic flow at high temperature ($\sim 10^6$ K) into supersonic flow at comparatively low temperature ($\sim 10^{4.5}$ K). From there on out, the flow

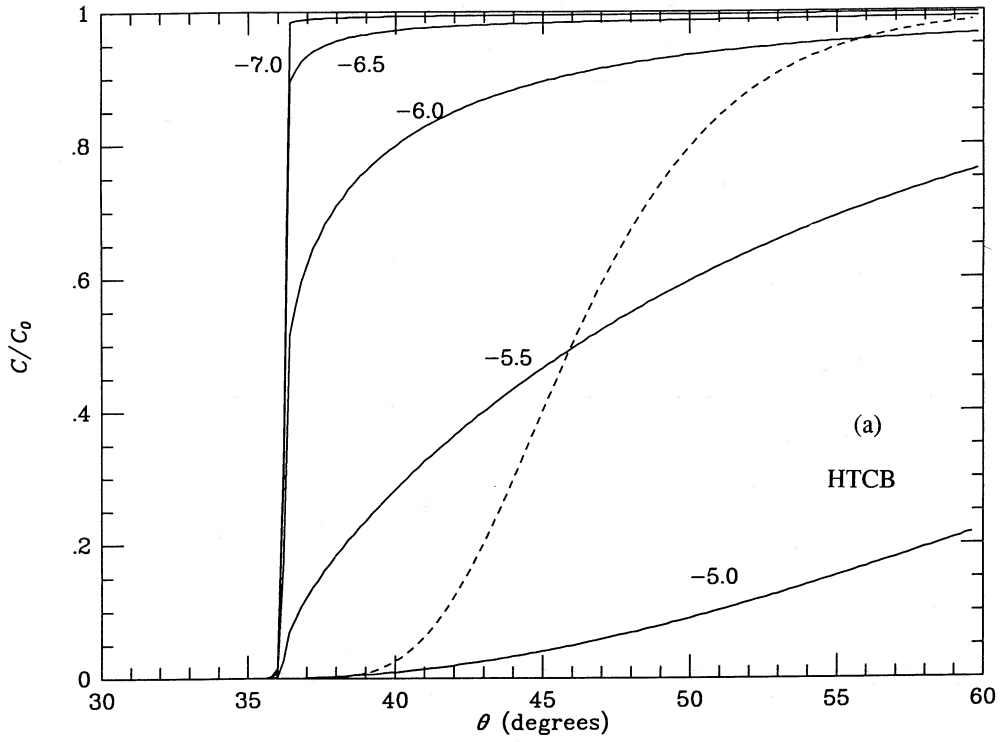

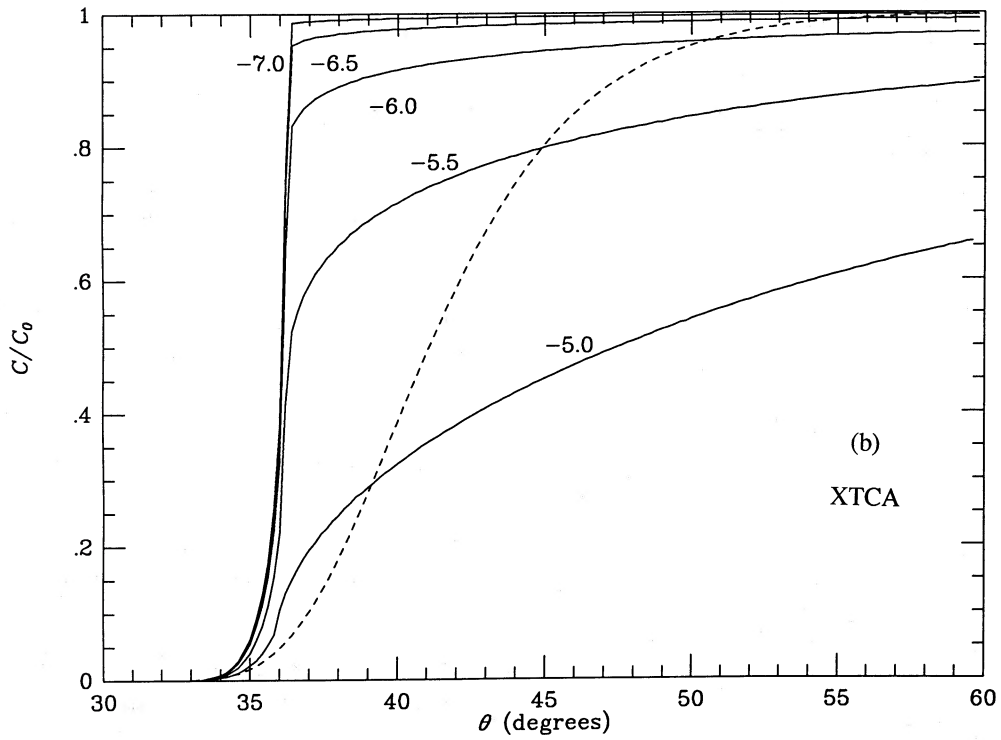

FIG. 11.—(*a*) Calculated eclipse transition curves (*solid lines*) for HTCB for a wind accelerated by a $1/r^2$ force, for various mass-loss rates and ionization by X-rays from Cen X-3 at an assumed X-ray luminosity of 10^{38} ergs s^{-1}. Curves are labeled by the logarithm of the mass-loss rate expressed in solar masses per year. Dashed line is the archetypal curve for $\theta_0 = 37°.2$ and $h = 6.3 \times 10^{10}$ cm. (*b*) Same for XTCA, except $\theta_0 = 32°.9$. (*c*) Runs of density (*solid lines: left scale*) and velocity (*dashed lines: right scale*) for the various assumed mass-loss rates.

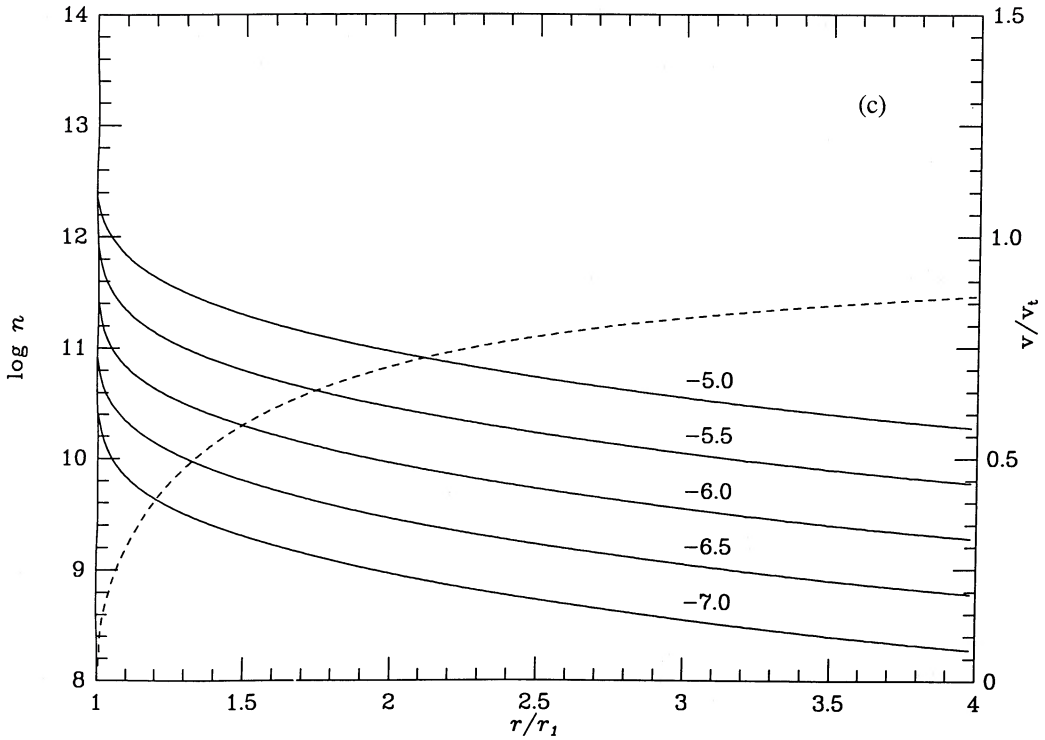

FIG. 11—*Continued*

is driven by radiation pressure with a velocity conforming to equation (24), where v_1 and r_1 are set equal to the values of the velocity and radius at the top of the coronal layer.

In a highly ionized corona the radiation force is caused almost entirely by Thomson scattering and has the same effect as a reduction in the effective gravity. For ionized hydrogen of atomic mass m at temperature T in the gravitational field of a star of mass M the equations of motion and continuity can be combined to obtain the flow equation

$$(1 - c^2/v^2)vdv + (\omega^2 r_1/r - 2c^2)dr/r = 0 , \qquad (26)$$

where $c = (2kT/m)^{1/2}$ is the thermal velocity,

$$\omega = [G(1 - \Gamma)M/r_1]^{1/2}$$

is the escape velocity at the radius $2r_1$, and Γ is the ratio of the magnitudes of the radiation force due to Thomson scattering to the gravity force. Setting $u = v/\omega$, $\tau = c/\omega$, and $z = r/r_1$, equation (26) becomes

$$[1 - (\tau/u)^2]udu + (1/z - 2t^2)dz/z = 0 . \qquad (27)$$

As before, we fix $n_1 = 4.5 \times 10^{12}$ cm^{-3} at the tangent point corresponding to $\theta = 36°$ where the earliest start of an observed XTCA transition curve occurs. We note that the temperature parameter τ is identical to the one defined previously to characterize the scale height of the hydrostatic density function; we set it to the value which gave a good fit for the hydrostatic density function, namely $\tau = 0.253$. The initial value of u at $z = 1$ is $u_1 = v_1/\omega$, which is set by the choice of the mass-loss rate. Figure 12 shows the calculated velocity curves for five values of the mass-loss rate from $10^{-7.5}$ to $10^{-5.5}$ $M_\odot$ yr^{-1}. The dashed lines show the runs of velocity that would be required to give the same mass-loss rates if the densities conformed to the hydrostatic density function for $\tau = 0.253$.

The critical point of the steady state solution to the flow equation lies far out at $r_1/2\tau^2 \sim 7.8r_1$. All solutions which start off with velocities high enough to achieve mass-loss rates typical of O-type supergiants reach the sonic point, where $(1 - \tau^2/u^2) = 0$, far inside the critical radius. We conjecture that this is where the coronal heating mechanism shuts off, the plasma cools rapidly, the flow becomes supersonic, and the radiation pressure takes over to complete the acceleration to the terminal velocity. The radius at which this transition occurs depends on the mass-loss rate, as indicated in Figure 12. A high value of the mass-loss rate implies a large value of the initial velocity, v_1, and a corresponding small value of the radius, r_2, at which the transition to the radiation-driven wind regime begins.

Figures 13*a* and 13*b* show the predicted eclipse curves for this hybrid corona wind model, and Figure 13*c* the runs of velocity and density for values of M in the range from $10^{-7.5}$ to $10^{-5.5}$ $M_\odot$ yr^{-1}. Values of $\dot{M}$ in excess of $10^{-6.5}$ $M_\odot$ yr^{-1} give transition curves which either have too rapid initial rises or approach their asymptotic values too slowly. The calculated transition curves for mass-loss rates less than this are in satisfactory agreement with the archetypal curves, both in shape and in the phase shift between the HTCB and XTCA transitions. We believe this agreement is evidence for the validity of the corona wind model, and, therefore, for the existence of a million degree coronal layer at the base of the stellar wind in KRZ, and an upper limit of $10^{-6.5}$ $M_\odot$ yr^{-1} on the mass-loss rate.

A corona of the thickness and temperature that our model requires has a very high luminosity in soft X-rays. We estimate its emission measure according to the formula

$$\mathrm{EM} = \int_{r_1}^{r_2} 4\pi\{r^2 n_1^2 \exp[-2(r - r_1)/(\tau^2 r)]\}dr , \qquad (28)$$

where r_2 is the radius at the top of the coronal layer. From Figure 12 we find $r_2 \sim 1.27r_1$ for $M = 10^{-6.5}$ $M_\odot$ yr^{-1}. The

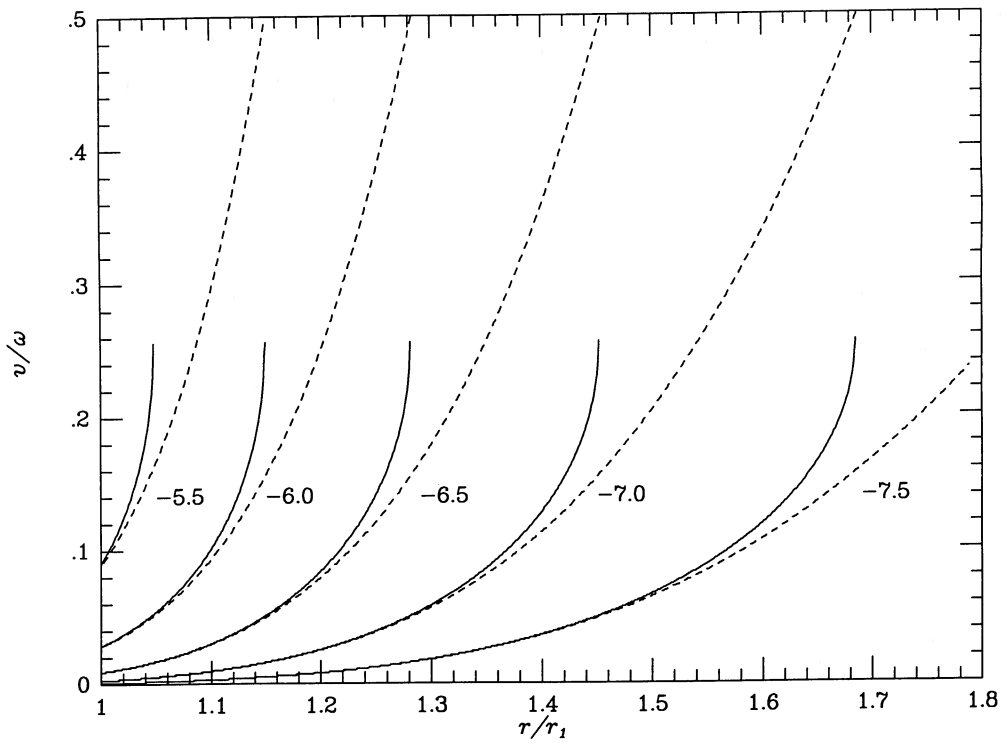

FIG. 12.—Plots of wind velocity vs. radius for various mass-loss rates. Solid lines are solutions of the hydrodynamic wind equation for $\tau = 0.233$. Dashed lines are velocity runs for the isothermal hydrostatic density function with a scale height of $\tau^2 r_1 = 4.9 \times 10^{10}$ cm. Curves are labeled by the logarithm of the mass-loss rate expressed in solar masses per year.

resulting emission measure is 4×10^{60} cm^{-3}. The total cooling coefficient Λ varies little over the temperature range 0.4–2.0 $\times 10^6$ K and is $\sim 4 \times 10^{-23}$ ergs cm^3 s^{-1} (Mewe *et al.* 1985). The result is a luminosity of 2×10^{38} ergs s^{-1}, $\sim 3\%$ of the bolometric luminosity of KRZ. Most of the coronal luminosity is in soft X-rays which is absorbed by the cool matter farther out and reradiated mostly in the far-UV. If the unspecified coronal heating mechanism turns off at $1.27r_1$, a rapid transition to the cool radiation-driven wind regime is assured by the fact that the cooling time for a cosmic plasma at $T = 10^6$ K at a density of $n = 10^{11}$ cm^{-3} is $kT/\Lambda n \sim 10$ s. In this time the wind moving at the coronal sound speed $c = (2kT/m)^{1/2} \sim 100$ km s^{-1} travels a distance of only $\sim 10^{-4} r_1$.

We have not yet explored the observable effects which the large luminosity of soft X-rays implied by our model may have. We note, however, that Baade and Lucy (1987) have argued against the existence of a hot coronal layer in the O-type star ξ Puppis on the basis of their observed upper limits on coronal line emission.

VI. CEN X-3 MASS

Estimates of the mass of the neutron star in an accretion-powered X-ray binary are generally based on the assumption that the companion star fills its Roche lobe. Under this assumption the orbital phase at which the occultation of an eclipsing binary X-ray source is just complete, called the eclipse half-angle, provides a measure of the Roche lobe radius with a range of possible values determined by the uncertainty in the inclination of the orbit. In the case of Cen X-3 the value of the eclipse half-angle itself has been quite uncertain due to the high degree of variability in the eclipse phenomena and the evident difficulty of identifying which feature of the eclipse transition curve is the appropriate measure of the "surface" of KRZ. Our observations in the XTCA channel probed the density function directly to values of $n \sim 4 \times 10^{12}$ cm^{-3} at the radius r_1 of the near point to the line of sight at $\theta = 36°$. Earlier we defined a "reference radius" at unit optical (i.e., X-ray) depth in the atmosphere. Fitting the parameters of the exponential density function to the observed transition data, we showed that the mean value of the corresponding "reference angle" is 32°.9. We believe this is a more accurate value of the "eclipse half-angle" which figures in the estimate of the Cen X-3 mass. One might ask whether the reference radius is a plausible estimate of the radius of the Roche lobe. An accretion-driven luminosity L_{38} (in units of 10^{38} ergs s^{-1}) from a neutron star of mass m_x (in units of $M_\odot$) and radius R_6 (in units of 10^6 cm) requires an accretion rate of

$$\dot{M}_{18} = R_6 L_{38}/1.33 m_x , \tag{29}$$

where the accretion rate is expressed in units of 10^{18} g s^{-1}. If the accretion flow is drawn from an area A where the density is n_0, then the flow velocity is

$$v_a = \dot{M}/(\mu n_a A) = (10^{18} \text{ g s}^{-1}) R_6 L_{38}/1.33 m_x \mu n_0 A , \tag{30}$$

where μ is the mean atomic mass. For $L_x = 10^{38}$ ergs s^{-1}, $m_x = 1.4$, $R_6 = 1$, $n_0 = 1.13 \times 10^{13}$ cm^{-3}, $\mu = 1.3 m_p$, and $A \sim 0.1 r_1^2 = 5 \times 10^{22}$ cm^2, one finds $v_0 = 4.6$ km s^{-1}, which is a plausibly small velocity. Thus we take 32°.9 as the value of the eclipse half-angle, corresponding to the line of sight that grazes the limb of KRZ at unit optical depth for ~ 10 keV X-rays.

Rappaport and Joss (1983) have made a comprehensive analysis of the masses of neutron stars in binary systems. In each case they carried out Monte Carlo calculations of the distribution of mass estimates derived from values of the

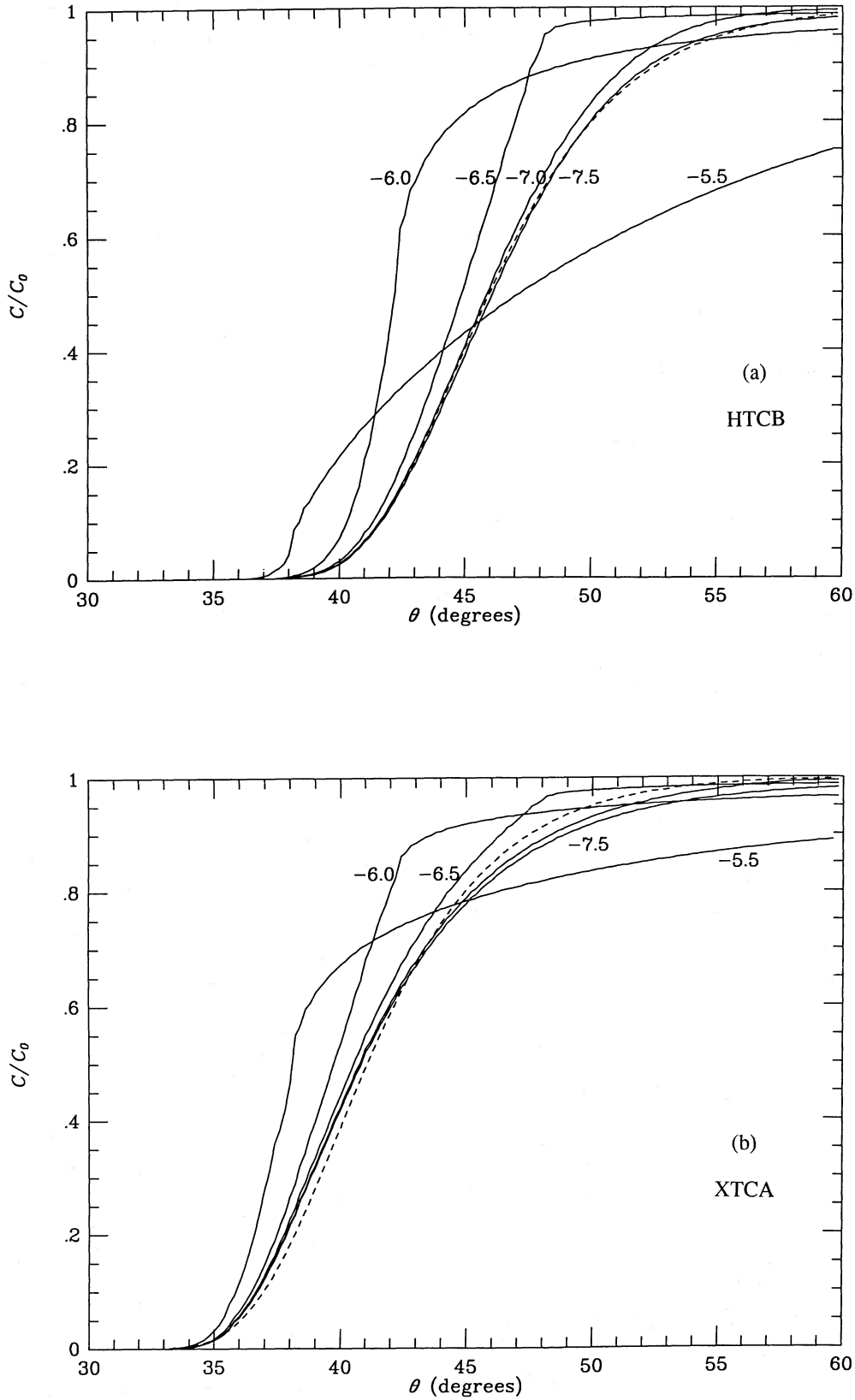

FIG. 13.—(*a*) Calculated eclipse transition curves for the HTCB channel for a hybrid corona wind model for various assumed rates of mass loss and ionization by X-rays from Cen X-3 at an assumed X-ray luminosity of 10^{38} ergs s^{-1}. Curves are labeled by the logarithm of the mass-loss rate expressed in solar masses per year. Dashed line is the archetypal curve for $\theta_0 = 37.^{\circ}2$ and $h = 6.3 \times 10^{10}$ cm. (*b*) Same for XTCA, except $\theta_0 = 32.^{\circ}9$. (*c*) Runs of density (*solid lines: left scale*) and velocity (*dashed lines: right scale*) for various assumed mass-loss rates.

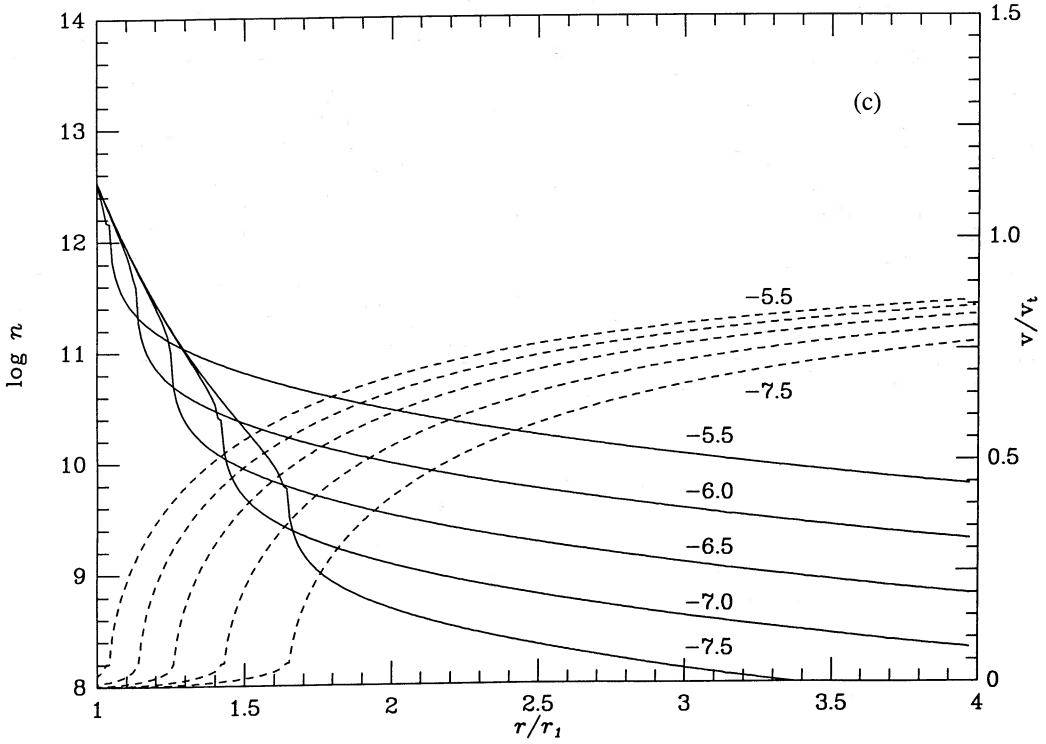

system parameters, each having an estimated error distribution. In the case of Cen X-3 they used values of the eclipse half-angle distributed uniformly in the range 35°–40° and derived a mass estimate (units of $M_\odot$) of 1.07(+0.63–0.57). Using their formulae, we find that a small change, $\Delta\theta_e$, in the assumed eclipse half-angle causes a change, $\Delta m_x = -(0.04\Delta\theta_e)$ $M_\odot$, in the derived mass of the neutron star. Thus a shift of $\sim -4\overset{\circ}{.}6$ from the midpoint of their range for the eclipse half-angle to our value of $32\overset{\circ}{.}9$ implies an estimated mass of the neutron star of $(1.23 \pm 0.60)\ M_\odot$. The overall uncertainty in m_x remains quite large. It could be reduced only by a refinement of the optical data on the amplitude of the velocity of KRZ and the inclination of the orbit.

VII. SUMMARY

1. We have measured 15 X-ray occultations of Cen X-3 by the atmosphere of its O-type primary KRZ over the energy range from 2 to 20 keV.

2. The data cannot be fitted by occultation curves computed for a KRZ atmosphere with a run of density implied by a purely radiation-driven wind.

3. The data are fitted well by occultation curves computed for a hybrid corona wind model in which it is assumed that the initial acceleration of the wind is caused by thermal pressure in a million degree coronal layer. Near the radius at which the wind velocity approaches the sound speed at the coronal temperature rapid cooling occurs, leaving the wind moving with a velocity that is supersonic at the lower temperature. Final acceleration to hypersonic velocities is caused by the conventional mechanism of radiation pressure.

4. The observed shapes of the X-ray occultation curves, interpreted according to the hybrid model, place an upper limit on the rate of mass loss of the order of $10^{-6.5}\ M_\odot\ \mathrm{yr}^{-1}$.

5. An estimation of the mass of Cen X-3, based on an improved measure of the eclipse half-angle derived from our data, yields $(1.23 \pm 0.60)\ M_\odot$.

Preliminary analysis of a portion of the data was carried out by Fuk Li. The authors thank Edward Morgan for generous advice and assistance in the use of the data analysis system, and Walter Lewin for a careful reading of the manuscript. They also thank Richard McCray for valuable suggestions. G. W. C. had useful discussions with Andrew Fabian and Martin Rees during a visit to the Institute of Astronomy, Cambridge, England. G. M. thanks the Government of China for support during his visit to MIT. This work was supported by NASA grant NAGW/442.

REFERENCES

Abbott, D. C., Bieging, J. H., Churchwell, E., and Cassinelli, J. P. 1980, *Ap. J.*, **238**, 196.
Baade, D., and Lucy, L. B. 1987, *Astr. Ap.*, **178**, 213.
Barlow, M. J., and Cohen, M. 1977, *Ap. J.*, **213**, 737.
Bennett, K., *et al.* 1976, *Astr. Ap.*, **51**, 475.
Bonnet-Bidaud, J. M., and Van der Klis, M. 1979, *Astr. Ap.*, **73**, 90.
Cassinelli, J. P., and Olson, G. L. 1979, *Ap. J.*, **229**, 304.
Cassinelli, J. P., Olson, G. L., and Stalio, R. 1978, *Ap. J.*, **220**, 573.
Cassinelli, J. P., Waldron, W. L., Sanders, W. T., Harnden, F. R., Rosner, R., and Vaiana, G. S. 1981, *Ap. J.*, **250**, 677.
Castor, J. I., Abbott, D. C., and Klein, R. I. 1975, *Ap. J.*, **195**, 157.
Chodil, G., Mark, H., Rodrigues, R., Seward, F., Swift, C. D., Hiltner, W. A., Wallerstein, G., and Mannery, E. J. 1967, *Phys. Rev. Letters*, **19**, 681.
Conti, P. S., and de Loore, C. W. H., eds. 1979, *IAU Symposium 83, Mass Loss and Evolution of O-Type Stars* (Dordrecht: Reidel).
Conti, P., and Garmany, C. D. 1980, *Ap. J.*, **238**, 190.
Fransson, C., and Fabian, A. C. 1980, *Astr. Ap.*, **87**, 102.
Giacconi, R., Gursky, H., Kellogg, E., Schreier, E., and Tananbaum, H. 1971, *Ap. J. (Letters)*, **167**, L67.
Hatchett, S., and McCray, R. 1977, *Ap. J.*, **211**, 552.

Hearn, A. G. 1975, *Astr. Ap.*, **40**, 277.
Hutchings, J. B., Cowley, A. P., Crampton, D., van Paradijs, J., and White, N. E. 1979, *Ap. J.*, **229**, 1079.
Kallman, T., and McCray, R. 1982, *Ap. J. Suppl.*, **50**, 263.
Krzemiński, W. 1973, *IAU Circ.*, No. 2612.
———. 1974, *Ap. J. (Letters)*, **192**, L135.
Lamers, H. J. G. L. M., and Morton, D. C. 1976, *Ap. J. Suppl.*, **32**, 715.
Lucy, L. B., and Solomon, P. M. 1970, *Ap. J.*, **159**, 879.
Lucy, L. B., and White, R. L. 1980, *Ap. J.*, **241**, 300.
Marlborough, J. M., and Roy, J. R. 1970, *Ap. J.*, **160**, 221.
McClintock, J. E., *et al.* 1976, *Ap. J. (Letters)*, **206**, L99.
Mewe, R., Gronenschild, E. H. B. M., and van den Oord, G. H. J. 1985, *Astr. Ap. Suppl.*, **62**, 197.
Morrison, R., and McCammon, D. 1983, *Ap. J.*, **270**, 119.
Morton, D. C. 1967, *Ap. J.*, **147**, 1017.
Nelson, G. D., and Hearn, A. G. 1978, *Astr. Ap.*, **65**, 223.
Parker, E. N. 1958, *Ap. J.*, **128**, 664.
———. 1965, *Space Sci. Rev.*, **5/6**, 666.
Pounds, K. A., Cooke, B. A., Ricketts, M. J., Turner, M. J., and Elvis, M. 1975, *M.N.R.A.S.*, **172**, 473.
Rappaport, S., and Joss, P. 1983, in *Accretion-driven Stellar X-Ray Sources*, ed. W. H. G. Lewin and E. P. J. van den Heuvel (Cambridge: Cambridge University Press), p. 1.
Rickard, J. J. 1974, *Ap. J. (Letters)*, **189**, L113.
Schreier, E., Levinson, R., Gursky, H., Kellogg, E., Tananbaum, H., and Giacconi, R. 1972, *Ap. J. (Letters)*, **172**, L79.
Schreier, E. J., Swartz, K., Giacconi, R., Fabbiano, G., and Morin, J. 1976, *Ap. J.*, **204**, 539.
Ulmer, M. P. 1976, *Ap. J.*, **204**, 548.
van Paradijs, J. 1983, in *Accretion-driven Stellar X-Ray Sources*, ed. W. H. G. Lewin and E. P. J. van den Heuvel (Cambridge: Cambridge University Press), p. 189.
Vidal, N. V., Wickramasinghe, D. T., Peterson, B. A., and Bessell, M. S. 1974, *Ap. J. (Letters)*, **191**, L23.
Waldron, W. L. 1984, *Ap. J.*, **282**, 256.
White, N. E., and Holt, S. S. 1982, *Ap. J.*, **257**, 318.
White, N. E., Swank, J. H., and Holt, S. S. 1983, *Ap. J.*, **270**, 711.

GEORGE W. CLARK: Room 37-611, MIT, Cambridge, MA 02139

GUOZHU MI: Department of Physics, Nanjing Aeronautical Institute, Nanjing, China

JOSEPH R. MINATO: 2151 Lakeview Road, Lakeview, NY 14085